J. Fluid Mech. (1989), *vol.* 209, *pp.* 151–190
Printed in Great Britain

Large-scale structure in the far field of buoyant jets

By DIMITRIS PAPANTONIOU[1] AND E. JOHN LIST[2]

[1] ETH - Hönggerberg, 8093 Zürich, Switzerland

[2] California Institute of Technology, Pasadena, CA 91125, USA

(Received 23 August 1988 and in revised form 10 February 1989)

The flow structure and entrainment mechanisms in the far field of a round vertical buoyant jet have been studied experimentally by use of an optical technique based on laser-induced fluorescence (LIF). A large number of essentially instantaneous tracer concentration profiles were recorded for each experimental run by combining LIF with linear photodiode array imaging and high-speed digital data acquisition. Analysis of the resulting high-resolution flow images indicates that the far-field region is dominated by the periodic passage of structures spanning the entire radial flow extent. Ambient fluid is entrained by vortical motions and is transported to regions deep into the flow interior. Correlation analysis discloses that the passage frequency of the structures scales with the local mean velocity and flow width. Conditional averaging of the data indicates that the downstream frontal region of the structure is well mixed and at a higher concentration level than the back and side regions where ambient fluid is intermittently present. This results in an axial concentration gradient within the structure, analogous to the ramp-like pattern previously observed in heated air jets. In comparison to the momentum-driven flow the ambient fluid presence in the flow interior is greatly increased when body forces are the driving mechanism. This appears to result from the influence of buoyancy forces in the production of turbulent vortices at the integral scale. An important feature of both the momentum-driven and buoyancy-driven flows investigated is the strongly intermittent character of the concentration field. This raises the issue of the appropriateness of gradient-diffusion theories for the description of such flows.

1. Introduction

Many flows in engineering practice and environmental science are either influenced by the presence of buoyancy or are driven entirely by forces derived from buoyancy. Although the geometry of flows nominally axisymmetric about a vertical axis is simple, which makes their experimental study relatively straightforward, there are nevertheless good reasons to study such flows and document their structure in every detail. They play an important role in understanding shear flow in general and their characteristics are of direct relevance in many engineering design problems, including dilution, mixing, and combustion.

This paper reports on an investigation of a round turbulent buoyant jet flow, which is the nominally axisymmetric flow field established by a source of momentum and buoyancy in an 'infinite' medium. A particular aspect of the flow we are concerned with is the effect of buoyancy on the structural characteristics of the concentration field of a passive scalar initially carried by the discharged fluid, at a large distance from the flow source where the flow is self-preserving. Although there have been a number of both experimental and theoretical studies of round momentum jets, and

a lesser number of plume studies (see Chen & Rodi, 1980; List 1982; Papanicolaou & List, 1988 for reviews), the majority of the experiments to date have centred on point measurements of the velocity components and the concentration of a passive scalar carried by the discharged fluid. The velocity components have usually been measured with hot-wire probes or laser-Doppler velocimeters. Measurements of the concentration have been performed with hot wires, thermistor probes, density probes and non-intrusive optical techniques, including light scattering, Raman spectroscopy, and laser-induced fluorescence (LIF). Emphasis has been placed on increasing the spatial and temporal resolution of the measuring devices to enable study of the smallest scales of flow. From these point measurements, a comprehensive view of the time-averaged characteristics of the turbulent buoyant jet flow field has emerged. These include velocity and concentration profiles, turbulent fluctuation intensity and shear stress profiles, as well as the gross entrainment characteristics. Papanicolaou & List (1988) reported recently on such measurements carried out in our facility.

Despite the large number of experiments that have been done, several aspects of the turbulent flow field relating to its instantaneous structure and possible organization still remain unclear. This is partly due to the complexity of the turbulent flow in general, and partly due to shortcomings of available experimental methods. It may also be attributed, as List (1982) has noted, to a preoccupation with time-averaging techniques. For example, while it is now well established that the near-field region of jet development is dominated by vortex dynamics, evidence of an analogous large-scale organization in the self-preserving region is not yet conclusive. Interest in the possible large-structure organization of the far field of turbulent jets and buoyant plumes has been fuelled by the large-scale flow organization apparent in the plane shear layer. During the last fifteen years, the work of Brown & Roshko (1974) has inspired a thorough investigation of the shear layer large-scale flow dynamics. Flow visualization and other field measurement techniques have proved to be very useful in revealing the flow structure, at least in this case where the flow is mainly two-dimensional. It is now widely recognized that such field measurements, while inherently more difficult to perform and generally less accurate than point measurements, are nevertheless capable of leading to an understanding of the complex turbulent flow processes.

The traditional view of turbulent structure and mixing in the far field of an axisymmetric jet has been that it is mainly composed of eddies, smaller than the lateral extent of the turbulent region, that evolve in a rather stochastic manner and which are responsible for the transfer of momentum and kinetic energy, as well as the entrainment of ambient fluid and subsequent mixing. This view, which has been based mainly on the results of point measurements, has lent some support to the notion that turbulence 'diffuses' and that local turbulent fluxes of various quantities are proportional to the local gradient of the corresponding average profiles. While numerical studies based on these models have some success in predicting profiles of averaged flow quantities, they have difficulty in predicting the mixing characteristics of shear flows (Walker 1979; Sreenivasan, Tavoularis & Corrsin 1981). Also, it is notable that most models of turbulent transport and mixing do not take into account the effects of the molecular diffusivity which characterizes the value of the Schmidt number ($Sc = \nu/D$). However Schmidt number effects seem to be important; the experiments of Konrad (1976), Breidenthal (1981), Mungal & Dimotakis (1984), and Koochesfahani & Dimotakis (1986) show that the amount of molecular mixing in gas

and liquid shear layers (at the same conditions otherwise) differs by a factor of two. Since the Schmidt number of a gas phase and liquid phase flow differ typically by more than two orders of magnitude, it follows that some caution should be exercised when comparing flow quantities associated with mixing at different *Sc*.

Broadwell & Breidenthal (1982), noting that mixing models based on the concept of gradient diffusion are inapplicable to turbulent shear layers, proposed a new simple model for mixing in such flows that incorporated the observed large-scale shear layer features and concepts from the Kolmogorov cascade in scales. Predictions based on their model are in qualitative agreement with recent experimental observations of mixing in the plane shear layer including Schmidt number effects (see Koochesfahani & Dimotakis 1986 for a discussion). Effelsberg & Peters (1983) incorporated similar concepts in a model of the probability density function (p.d.f.) of a passive scalar. Their model p.d.f., quantitatively different from the p.d.f.'s traditionally used in combustion modelling, attempts to quantify the individual contributions of the 'turbulent', 'ambient', and 'interface' regions in a mixing layer and was supported by measurements of Drake, Pitz & Shyy (1986) in a turbulent jet diffusion flame.

During the last decade, a growing number of investigators have attempted to establish the existence of a large-scale organization in axisymmetric shear flows and document the characteristics of such an organization. The measurements of Antonia, Prabhu & Stephenson (1975) and Sreenivasan, Antonia & Britz (1979) make it clear that large-scale motion plays an important role in the heat and momentum transport in the intermittent (off-centreline) region of the far field in a round momentum jet. Chevray & Tutu (1978), from conditional measurements, detected the directions of fluid motion in the 'turbulent' and 'irrotational' regions and Zaman & Hussain (1984) found clear evidence of large structures in the axisymmetric shear layer formed by a jet discharge. Komori & Ueda (1985), from conditionally sampled two-point measurements in the far field of the momentum jet, also detected large coherent eddies with a vortical structure consisting of strong outward turbulent motion from inside the jet, turbulent reverse flow, and entrainment inflow in the irrotational ambient region. As the comprehensive review by Hussain (1986) makes very clear, there is no doubt whatsoever that turbulent shear flows in general contain organized motions.

It is a fact that virtually all of the quantitative studies of this nature have been performed in gas-phase momentum jets. As already mentioned, quantities associated with mixing, such as the p.d.f. of scalar concentration and its moments, are expected to have a dependence on *Sc* which has not yet been established for round jets and plumes. The results of Sawford & Hunt (1986) suggest that the effect of molecular diffusion may be quite pronounced; they estimated a 2-fold increase in scalar fluctuation intensity for a 100-fold increase in *Sc*.

To date, there have been no investigations exploring the possible large-scale organization of turbulent buoyant plume flows. There are also no measurements that can explore the effect of buoyancy on the instantaneous shear flow structure. Some photographic evidence in the work of Kotsovinos (1977) suggest a possible flapping mode for the far-field plane plume. It is of interest that Uberoi & Singh (1975) who obtained spatially correlated measurements (instantaneous profiles) by projecting a hot-wire probe at right angles to the flow direction, observed such a mode for the plane jet.

The experiments reported here were aimed at both a qualitative and a quantitative

study of the entrainment and mixing characteristics of a round buoyant jet. They were also intended to determine the degree of large-scale organization in a turbulent flow driven by buoyant forces, and to document its main features. The cases of a liquid-phase pure momentum jet and a buoyancy-driven plume were studied. Experiments covered the range from near the jet exit to 150 exit diameters downstream, at a Reynolds number up to 10000 for the turbulent momentum jet. For the case of the buoyant plume, the experiments were carried to large axial distances where the initial momentum flux plays no apparent dynamic role and the flow is entirely driven by buoyancy forces.

The analysis is based on experiments in which the instantaneous concentration field was studied quantitatively by use of a laser-induced fluorescence (LIF) technique, which yielded temporally and spatially correlated measurements of the concentration of a passive scalar (a fluorescent dye) premixed with the discharged fluid. Each experiment provided a long time series of the instantaneous fluorescence light intensity emitted by dye molecules in a volume illuminated by a laser beam. Individual realizations consisted of essentially simultaneous measurements along the laser-illuminated line in the flow, which was imaged to a scanned linear photodiode array whose output was digitized and recorded in real time by a high-speed data acquisition system. This system, developed during the course of the experiments, is capable of continuously acquiring successive LIF measurements at a sufficiently high rate to 'freeze' the turbulent motion across the extent of the flow under consideration. The fluorescence intensity values were converted to local scalar concentration values by a simple procedure introduced by Koochesfahani (1984). Subsequent analysis of these highly resolved measurements enabled the study of the detailed structure of the scalar concentration field of both buoyant jet and plume flows which forms the basis of this paper.

2. Visualization of mixing in jets and plumes

Flow visualization is often the best method of gaining insight into turbulent mixing processes. The initial phase of this work deals with the static visualization of flow structures within turbulent momentum jets and buoyant plumes under various flow conditions. Important flow features are revealed that motivate the subsequent quantitative study of the concentration field by means of laser-induced fluorescence imaging with a photodetector array.

2.1. *Laser-induced fluorescence*

Laser-induced fluorescence (LIF) has been used primarily as a method for obtaining direct visualisation of the concentration field of a passive scalar in mixing and dilution problems where the fluorescing dye is premixed with one of the mixing species. Since the dye molecules (Rhodamine-6G or sodium fluorescein), which are highly soluble in water, fluoresce rather strongly when excited by laser light of the appropriate wavelength, dilution can be monitored down to scales as small as the spatial extent of excitation. The temporal resolution of the observation depends only on the integration due to the monitoring/recording system, since the time for fluorescence 'turn-on' is typically of the order of a few nanoseconds. Qualitative observations in shear flows using the LIF technique with photographic film as the recording medium were first made by Dewey (1976); lately the use of the technique has spread to a variety of flows. High spatial resolution is obtained by the use of planar light with a sheet thickness of the order of a millimetre. The temporal

resolution is controlled by the time of film exposure. Still LIF photographs of a round jet taken at a high spatial and temporal resolution by Dimotakis, Miake-Lye & Papantoniou (1983), showed that unmixed ambient fluid is transported deep within the flow region, suggesting that the far-field jet entrainment is dominated by large vortical structures. They observed concentration fronts spanning the entire flow width, and that the concentration along the flow axis does not decrease monotonically but rather in discrete steps corresponding to these advancing concentration fronts. Additional qualitative LIF observations in jets, largely confirming their observations, were made by Papantoniou (1985) and Dahm (1985), who also employed a chemically reactive LIF technique to study the mixing on a molecular scale. Shlien (1987) used LIF to study the dispersion of the entrained fluid by the main jet flow. He observed that the ambient fluid was engulfed by the large-scale structures and that entrained fluid crossed the jet centreline before being convected even a fraction of the local jet diameter.

Quantitative measurement using LIF and photographic recording is difficult (Shlien 1987), mainly due to the inherent limitations of film as the recording medium. A superior alternative for quantitative LIF measurements has been offered by the use of self-scanning linear, or planar, photodiode arrays to record the fluorescence resulting from laser line or planar illumination of the flow field. Dimotakis *et al.* (1983) illuminated the jet flow axis with a laser beam and used a 1024 element linear photodiode array to study features of turbulent jet entrainment. By using the output of the array to modulate the intensity of an oscilloscope beam that was driven in a raster scan fashion, and photographing the pattern directly off the oscilloscope screen, they recorded analog time–distance fluorescence intensity data.

An important contribution to the method was made by Koochesfahani (1984) who, using a linear array and line illumination, digitized and recorded time series data of fluorescence intensity in a shear layer flow, and introduced a method for determining accurately the local scalar concentration from the intensity data.

There are major advantages offered by the LIF visualization method over conventional methods. LIF makes it possible to 'slice' through the turbulent flow and obtain an instantaneous concentration pattern at a spatial resolution dictated by the light sheet thickness and the imaging optics. A time resolution adequate to freeze the turbulent motions is achieved by use of a short enough time exposure of the photographic film. It should be noted that, since the flow scales generally increase with increasing axial distance, the resolution is actually increasing along the axis of the flow. Thus, to visualize the flow over a large axial range at adequate resolution, the flow scale size can be varied by adjusting the nozzle diameter and Reynolds number.

It should be stressed that the resolution limit of the observation is an important issue. Most of the conventional flow visualization studies that have relied on back lighting, and used smoke or dye to render the turbulent mixing regions visible, have missed significant features of the entrainment process. These methods, offering an external or integrated view of the flow region, have suggested that it is in fact possible to define an interfacial surface that separates the 'turbulent zone' from the 'non-turbulent' one. Indentations of this surface, not actually visible with conventional techniques but measured by point probes, have been dealt with by use of the concept of intermittency. This was originally defined by Corrsin & Kistler (1955) in terms of the fluctuating vorticity, as the fraction of *the time a particular* point spends inside the 'turbulent zone'. The above ideas have supported a traditional description of the turbulent entrainment process (and the related mixing

and dilution) in terms of the diffusive, random-walk propagation of this interface into the irrotational, ambient fluid region (Townsend 1976). However, as indicated from typical LIF photographs of jets and plumes (figures 1–3) as well as from other published photographs (Dimotakis *et al.* 1983; Dahm 1985) this description of the entrainment process is not applicable to jet flow. Such photographs make it clear that the interfacial surface, if one can be defined, is topologically very complex and that ambient fluid is transported, relatively unmixed, by large vortical motions to regions deep within the jet.

2.2. *Buoyant jets and plumes*

Photographs of buoyant plumes visualized by LIF are presented in figure 1 (*a–d*). The plume is discharging from a 1 cm diameter nozzle at the middle of a tank (see Papanicolaou & List 1988 for physical details). The plume fluid is a solution of ethanol in water and the ambient fluid is a sodium chloride solution. The initial density difference is 1%, but refractive indices of the fluids are matched using the method of Hannoun & List (1988). The photographic exposure time is 17 ms and the light sheet thickness is about 0.5 mm. Approximately 75 exit diameters are imaged on film. In figure 1 (*a*), the valve controlling the flow rate was shut, so plume fluid is drawn vertically upwards from the source entirely by buoyancy forces. The flow resembles the familiar smoke plume from a burning cigarette, except that here LIF permits observation of regions in the plume 'interior'. This flow bears some resemblance to the flow pattern of a low-Reynolds-number jet, such as that presented in figure 1 (*d*) for a comparison. If L is the width of the plume flow field, then scales as small as $L/10$ are actively entraining ambient fluid, as evidenced by the continuous intertwining of the interfaces. This results in the higher degree of dilution that is expected in a plume flow on dimensional grounds (Fischer *et al.* 1979). In the plume flow case high values of the local concentration also imply a locally stronger density difference, to the extent that the differences in the molecular diffusion coefficients of dye, salt, and alcohol can be neglected. However, since all the molecular diffusion timescales are much longer than any turbulent timescale, these differences are of no consequence here.

Figure 1 (*b*) and (*c*) are LIF-based still photographs of a forced plume. Fluid at an initial density difference of 1% is discharged with an initial velocity of 10 cm/s. The ratio of the momentum length ($L_Q = 0.9$ cm) to the buoyancy lengthscale ($L_M = 3.2$ cm) gives an initial Richardson number $R_0 = 0.28$, (see Fischer *et al.* 1979 for a discussion of relevant lengthscales). Therefore, the results of Papanicolaou & List (1988) would indicate that the momentum jet-like character of the flow is lost after a distance $x/L_M = 5$, and predict a plume-like behaviour for $x/d \geqslant 20$. This should be compared to the pure jet flow in figure 2, which offers a simultaneous sectional view of the jet on two perpendicular planes intersecting on the axis; 27 exit diameters are imaged and the Reynolds number based on exit diameter of 2.54 cm is 8500. Discreet concentration 'fronts' observed simultaneously in both views are spanning almost the entire width of the flow. It may be observed that the plume flow is significantly more intermittent than the jet flow.

The visual change in behaviour from jet-like flow to plume-like flow appears gradual, notwithstanding the relatively rapid transition found in the measured mean velocity and concentration profiles (Papanicolaou & List 1988). Spade-like structures characteristic of the momentum jet can be discerned in the initial region of figure 1 (*b*). While the large-scale features of the momentum jet flow have their counterpart in the developed plume region, apparent differences develop in the smaller-scale

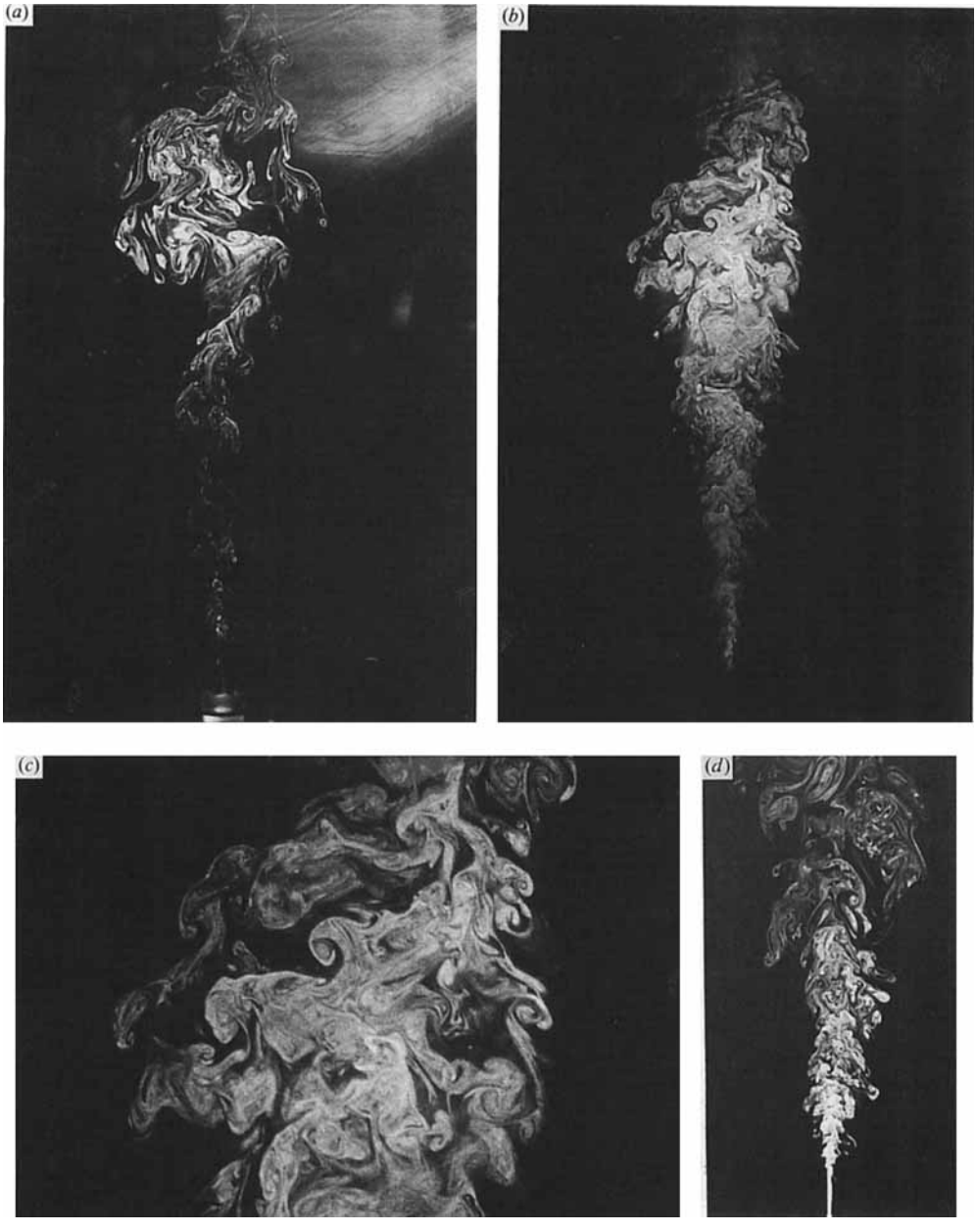

FIGURE 1. Laser sheet illumination photographs of plume and jet mixing. (*a*) Buoyancy-driven plume, (*b*) forced plume, (*c*) close up of plume flow in the far field, (*d*) jet at $Re = 700$, $0 < x/d < 700$.

structure of the concentration field. In comparison with figure 2, it may be observed that a different characteristic of the buoyancy-dominated flow compared to the momentum-dominated flow is the relative importance of smaller scales in the entrainment process. Figure 1(*c*) depicts an enlarged portion of the buoyant flow regime and a sharp concentration front is observed to span a large portion of the radial extent of the layer. Clearly, more ambient fluid can be found in the plume

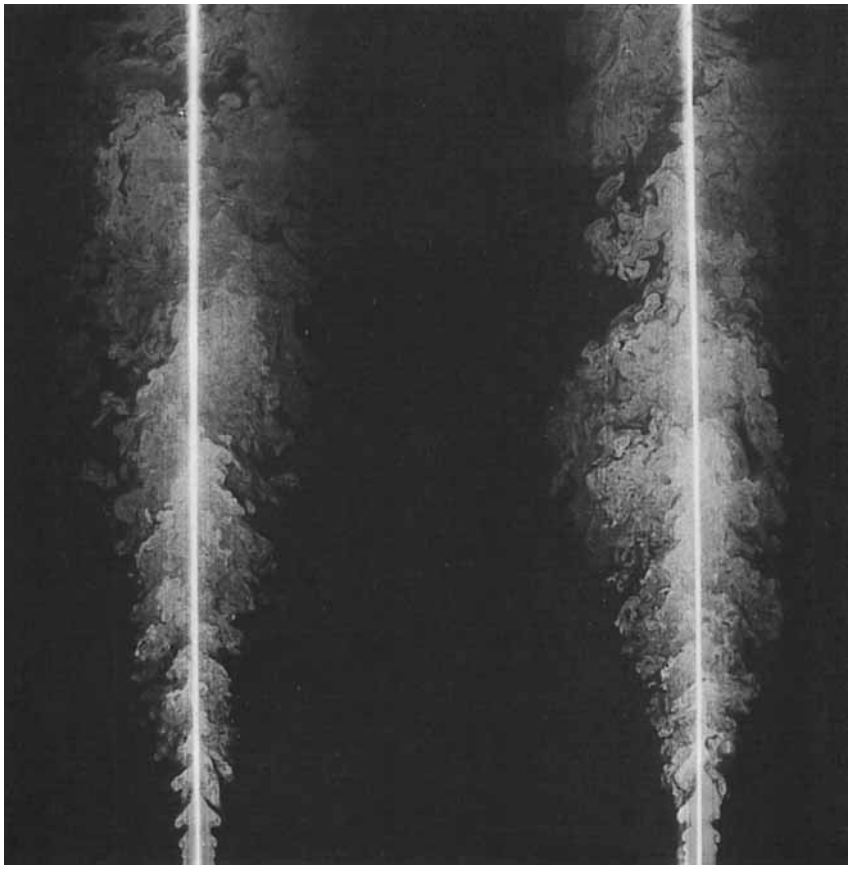

FIGURE 2. Simultaneous orthogonal views of jet mixing obtained from sheets of illumination intersecting on the jet axis, $Re = 8500$.

interior than in the jet. This observation is consistent with the high r.m.s. values of turbulent concentration and high intermittency throughout the plume regime measured by Papanicolaou & List (1988) and Kotsovinos (1977). The sharp concentration fronts and the abundance of ambient fluid in the plume interior are important features of the plume flow, indicating that entrainment into the plume region is achieved by large-scale motions. A feature that is related to the increased efficiency of the entrainment and mixing mechanism of the buoyant flow is the large variation of concentration level occurring over small scales, particularly over the braids of the apparent winding vortices. It should be noted here that the characteristic timescale for entrainment and mixing in a plume depends on axial distance differently than in a momentum jet. At distance x from the source, the local convection velocity U_c and the width of the flow L, define a large-scale time $T = L/U_c$. Dimensional considerations (Fischer *et al.* 1979) imply that for a momentum-driven jet $L = \alpha x$, for some constant α, and $U_c \approx 7.0 M^{\frac{1}{2}}/x$, where M is the specific momentum flux of the jet. These give an estimate for the large timescale for a jet:

$$T_j \approx 0.14 \alpha x^2 / M^{\frac{1}{2}}.$$

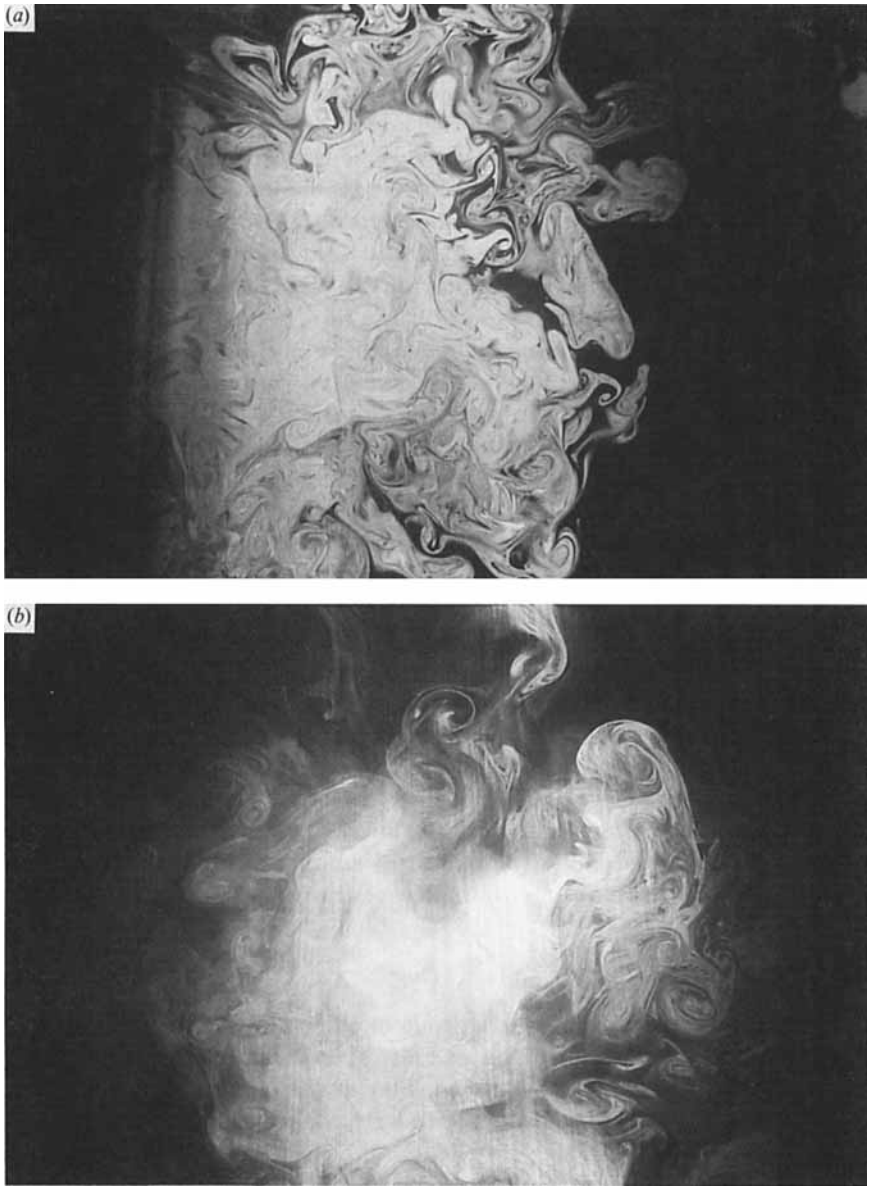

FIGURE 3. Sheet illumination photographs normal to the flow axis. (*a*) Jet mixing at $Re = 5600$, $x/d = 66$, (*b*) plume mixing at $x/L_M = 18$.

For a plume with local lengthscale $L = \alpha x$, and with axial velocity scale $U_c \approx 4.0(B/x)^{\frac{1}{3}}$, where B is the specific buoyancy flux, an upper estimate for the timescale is given by

$$T_p \approx 0.25\,\alpha x^{\frac{4}{3}}/B^{\frac{1}{3}}.$$

Note that this scaling depends on the selected eddy size through the angle parameter α (typically $\alpha = 0.4$ for both jets and plumes). For scales smaller than $L = \alpha x$, that participate in the entrainment/mixing process while essentially convecting at the same velocity as the large scales, an accordingly smaller timescale

for entrainment should be expected. It is also notable that the characteristic time for entrainment at a certain axial distance is much smaller when buoyancy rather than momentum is driving the flow, generally implying faster mixing. This characteristic of the buoyant flow is reflected in the mean concentration decay laws.

Finally, we should mention that the cascade in scales may proceed in a different manner when buoyancy is driving the flow. A density difference between the eddy and its environment gives rise to a body force proportional to the eddy volume that tends to accelerate it. Shear forces are generated as a result of body forces. If scales down to $L/10$ are dominant, this would imply that buoyancy affects the cascade process (and the energy density spectrum) by a direct input of energy at wavenumbers greater than $1/L$ imposed by the flow geometry.

Further insight into the entrainment mechanism, is presented by photographs of a transverse plane (perpendicular to the axis) appearing in figure 3(*a*, *b*). The Reynolds number for the momentum jet (in figure 3*a*) was 5600, based on the exit diameter of 1 cm. The plume operating conditions for the flow in figure 3(*b*) were similar to those of the flow in figure 1(*b*). In both cases, the transverse plane was located at an axial distance of 66 cm from the flow source (1 cm diameter). The light sheet thickness is comparable with that of the previous photographs.

A striking feature of such high-resolution photographs of the jet flow is that the concentration level over a centrally located flow area is markedly higher than that of the surrounding region. The position of this portion of the jet was observed (from time sequence photographs not shown here) to vary in time, implying the passage of large structures through the axial location illuminated by the sheet. There is a high degree of regularity in the time evolution of this phenomenon, which will be examined subsequently. A feature of the plume flow, which may also be observed in the enlarged axial view of figure 1(*c*), is the very large variations in concentration level associated with the intertwining of interfaces. The shape of some interfaces also appears to imply the existence of substantial smaller-scale vorticity in the axial direction, resulting in a three-dimensionality of the flow.

3. Dilution measurements

The dilution experiments were carried out in the jet facility of Keck Laboratory documented in detail in Papanicolaou & List (1988). The tank has a square cross-section (115 × 115 cm) and depth of 335 cm. The flow source was located at a distance of 100 cm from the bottom, and observations were conducted at a maximum distance of 115 cm from the source. Nozzles of 0.5 cm and 1 cm were used. The supply system is of the constant-head type, with a flow meter to control the volume rate. Buoyancy-driven flows were set up by placing a sodium chloride solution in the tank and then discharging a weak solution of ethanol in water from the nozzle (vertically upwards). A typical initial density difference of 1% was enough to ensure a buoyancy-driven flow far enough from the flow source. The refractive indices of the fluids, measured by a refractometer were precisely matched for all the dilution experiments.

The LIF system used for the quantitative measurements of concentration and dilution is documented in detail in Papantoniou (1985). We will briefly summarize here some of its features relating to the measurements to be presented. The 488 nm line from a 2 W argon-ion laser, focused by a 2 m focal length converging lens, was directed to intersect the flow in the radial direction. Fluorescein dye was premixed at a concentration of the order of 10^{-6} molar with the discharged fluid. The initial concentration was chosen so that the concentration maximum at the axial station

under observation was of the order of 10^{-7} molar. When excited by the laser light, the dye molecules emit light strongly in the yellow–green portion of the spectrum. A light orange filter was placed in front of the Reticon array camera to block the scattered blue laser light in the test section, while allowing a considerable portion of the green fluorescence signal to be measured. It was found that this combination resulted in the most efficient use of the available laser power, which for some measurements was limited to 800 mW. An Etalon assembly and a beam-stop were used to confine the beam to its TEM_{∞} mode; this resulted in a laser beam with a Gaussian intensity that was focused to about 500 μm diameter in the test section. Since the beam diameter defines the local measuring volume, it also defines the degree of spatial resolution (normal to the direction of propagation) attainable by the technique.

The fluorescing section of the laser beam was imaged by a 50 mm Nikon lens onto the sensitive area of a photodiode camera array (Reticon 300-A), containing 1024 photodiodes spaced 25 μm apart. By scanning the array at high speed and recording its output, virtually continuous profiles of fluorescence intensity were obtained along the line of the laser beam. The voltage output from each array 'pixel' is proportional to the integrated fluorescence intensity incident on the pixel during the line scan time. Since typically a 38 cm section of the laser beam was measured on the array, the spatial resolution for each pixel in the direction of beam propagation was generally of the order of 400 μm. The line scan time is analogous to the exposure time in conventional photography and it controls the temporal resolution of each individual measurement (pixel). This time is actually 1024 times the clock period (plus an adjustable number of blanking periods between scans). The appropriate line scan time for an experiment was chosen so that the temporal resolution was sufficient to resolve the fastest variations, corresponding to the local Kolmogorov passage time (see next section). Line scan times of up to 11 ms were used. The recording system consisted of a custom-made fast 8-bit ADC channel interfaced to the DMA port (DR11-B) of a PDP-11/60 computer and the associated software running under the RT11 operating system. The digitized data were continuously output to a 7 Mb Winchester disk (DSD-80). The input (to memory) and output (to disk) DMA processes were synchronized by controlling both interrupting devices in a double buffering scheme. The sustained throughput of the system was enough to record successive scans, with all 1024 pixels per scan, at a rate of 120 Hz per pixel.

At other times higher scanning rates were obtained by discarding one or more pixels for each pixel recorded, or one or more scans for each scan recorded, or both. Since the line scan time is not altered by this practice, there is no compromising the resolution of each individual measurement. The system was calibrated thoroughly before the experiments and the overall signal-to-noise ratio was quite high (over 200). It was subsequently used for other measurements in our facility, where the application was to turbulent mixing across horizontal density interfaces (Hannoun & List 1988).

3.1. *Sampling the concentration field*

The existence of characteristic timescales and, correspondingly, of physical frequencies in the flow field, demands that certain guidelines must be followed when sampling the concentration field of the turbulent buoyant flow. In particular, the length of the sample record and the sampling interval must be selected on the basis of the characteristic timescales in the flow.

The large-scale time for a certain axial location depends on the convection velocity

as indicated in §2. The measurements of Wygnanski & Fiedler (1969) suggest that the convection velocity is approximately equal to the mean centreline velocity, so a more precise estimate can be written (using values recommended in List 1982) as

$$T_j = 0.066\left(\frac{d}{U_0}\right)\left(\frac{x}{d}\right)^2,$$

where U_0 is the jet exit velocity.

For the buoyancy-driven plume the convection velocity can be estimated from concentration profiles taken along the plume axis (see §4.6 below) and it is approximately equal to the mean centreline velocity. Scaling laws then imply, using $U_c = 3.5\ (B/x)^{\frac{1}{3}}$, as suggested† in the review article of Chen & Rodi (1980), and with $\alpha \approx 0.4$, that

$$T_p = 0.1B^{-\frac{1}{3}}x^{\frac{4}{3}}.$$

The large-scale time at a particular axial station is related to the passage time of the large-scale eddies of the flow as seen by a probe fixed at this location. It has also been termed 'large-eddy turnover time' by some authors. Since the lowest frequency that is expected to exist in the flow is of the order of $1/T$, it is implied that the sample record time should be large enough compared with T for the formation of statistically stable estimates and the resolution of the lowest frequencies. The minimum sample record should be determined experimentally. From initial experiments, it was found that records spanning a minimum of $10T$ to $20T$ were necessary to obtain stable estimates of various statistical quantities.

At the smallest scales of the flow the important parameters are the viscosity and the rate of dissipation of kinetic energy (i.e. the rate at which mechanical energy is converted to heat). The Kolmogorov lengthscale is defined via these parameters by

$$\lambda_\nu = \nu^{\frac{3}{4}}/\epsilon^{\frac{1}{4}}.$$

The timescale pertinent to the Kolmogorov lengthscale is given by

$$t_\nu = (\nu/\epsilon)^{\frac{1}{2}}.$$

The implication of the concept of the Kolmogorov cascade in turbulent scales by which kinetic energy is transferred from scale L to scale λ_ν is that

$$\epsilon \sim U_c^3/L.$$

In other words, although the dissipation is ultimately due to viscosity, the order of magnitude of ϵ may be determined by those quantities that characterize the large eddies. Thus, the Kolmogorov scale is related to the large scale L and the Reynolds number Re through

$$\lambda_\nu \sim L/Re^{\frac{3}{4}}.$$

The characteristic small-scale time is also related to T by

$$t_\nu \sim T/Re^{\frac{1}{2}}.$$

This timescale is indicative of the fastest variations in the turbulent flow as related to the random, jittery motion of the smallest eddies. In a mixing flow where one of the species is labelled with a passive scalar, the small timescale is intimately connected to the motion of the thinnest interfaces. For flows at high Sc, little

† Recent measurements by Papanicolaou & List (1988) give a value of 3.85 for the numerical constant.

Initial conditions					
Reynolds number (nominal)...	5600	5600	5600	5600	9000
Jet nozzle diameter (cm)...	1	1	1	0.5	1
Local conditions					
Axial distance, x/d	48.5	75	105	150	105
Mean centreline velocity (cm/s)	6.9	4.5	3.2	4.5	5.1
Kolmogorov scale estimate (mm)	0.30	0.46	0.65	0.46	0.45
Small scale time estimate (s)	0.04	0.09	0.17	0.09	0.09
Large scale time estimate (s)	2.8	6.7	13.1	6.7	8.2
Kolmogorov passage time (ms)	4.3	10.4	20.2	10.4	8.9
Length imaged on array (cm)	38.9	38.9	38.9	41.5	38.9
Static resolution per pixel (mm)	0.38	0.38	0.38	0.40	0.38
Array clock period (ms)	6.02	4.00	10.04	9.99	10.04
Line scan time (ms)	6.31	4.20	11.16	10.31	11.17
Pixels/scan recorded	512	256	512	1024	512
Recording interval (ms)	12.62	16.78	22.33	41.26	11.17
Number of scans recorded	10240	20480	10240	5120	10240
Experiment duration (s)	129.3	343.7	228.6	211.2	114.4

TABLE 1. Experimental parameters for jet experiments.

Initial conditions		
Reynolds number (nominal)...	1000	1600
Jet nozzle diameter (cm)...	1	1
Richardson number...	0.28	0.20
Local conditions		
Axial distance, x/d	105	105
Mean centreline velocity (cm/s)	3.3	3.7
Kolmogorov scale estimate (mm)	0.63	0.58
Small scale time estimate (s)	0.40	0.34
Large scale time estimate (s)	12.7	11.3
Kolmogorov passage time (ms)	19.0	15.7
Length imaged on array (cm)	38.9	38.9
Static resolution per pixel (mm)	0.38	0.38
Array clock period (ms)	9.98	9.98
Line scan time (ms)	10.61	10.61
Pixels/scan recorded	1024	1024
Recording interval (ms)	42.43	42.43
Number of scans recorded	5120	5120
Experiment duration (s)	217.24	217.24

TABLE 2. Experimental parameters for plume experiments.

molecular mixing does occur until the even smaller Batchelor lengthscale is reached (Batchelor 1952, 1959). This scale is given by

$$\lambda_D = \lambda_\nu / Sc^{\frac{1}{2}}$$

It is at the Batchelor scale that fluid interfaces are actually smoothed by the action of molecular diffusion. Since the Schmidt numbers for gases and liquids differ by more than two orders of magnitude, differences in the amount of molecular mixing may be expected (Broadwell & Breidenthal 1982; Sawford & Hunt 1986). In any

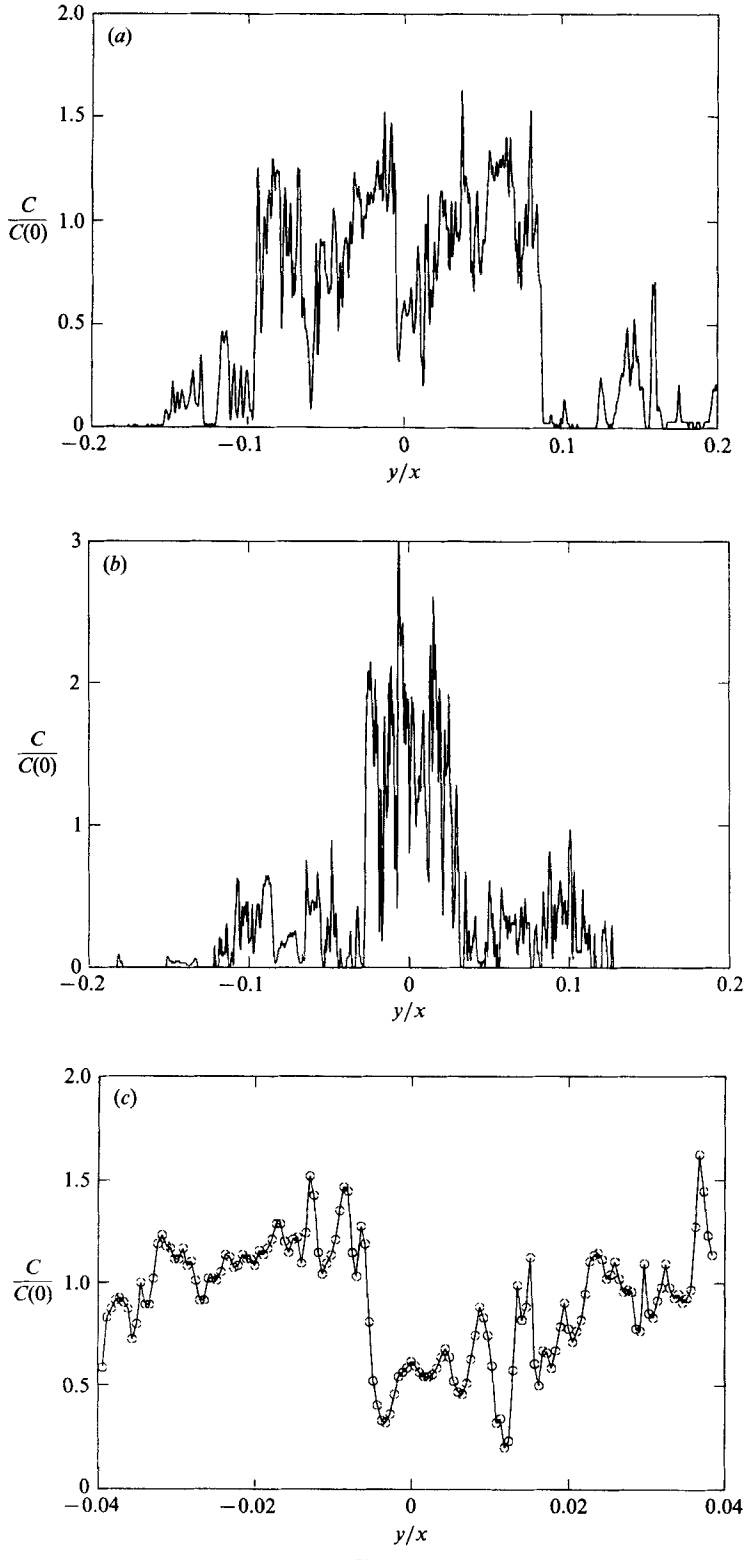

FIGURE 4 (*a–c*). For caption see facing page.

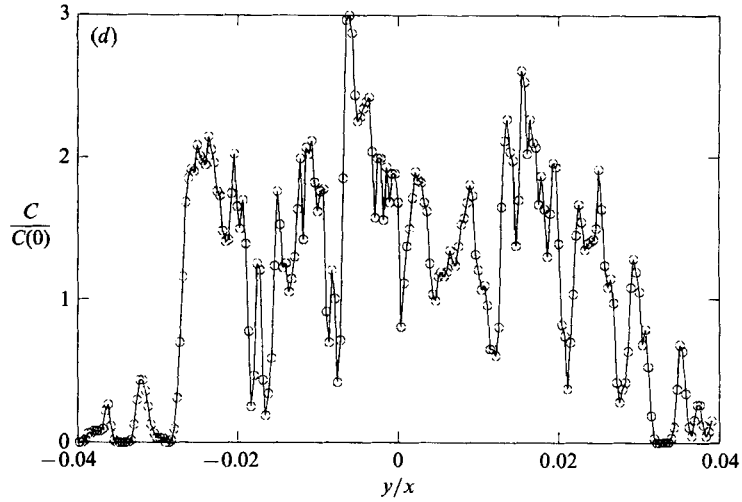

FIGURE 4. Instantaneous concentration profiles. (*a*) Jet at $Re = 5600$, $x/d = 150$. (*b*) Plume at $x/L_M = 24$, $x/d = 105$. (*c*) Detailed concentration profile for a jet at $Re = 5600$, $x/d = 150$. (*d*) Detailed concentration profile for a plume at $x/L_M = 24$, $x/d = 105$.

case, the implication is that at a high value of Sc, the interfaces remain sharp at scales comparable with the Kolmogorov scale. This was actually confirmed by the results to be presented subsequently.

The above considerations indicate that if the measurements are to resolve the scalar field at scales comparable with λ_ν and t_ν, then the minimum spatial and temporal resolution of the probe should be given by these scales. Further, if the flow pattern convects with a mean velocity of U, the sampling frequency necessary to 'freeze' the thinnest interfaces would be given by U/λ_ν. This frequency, associated with the Kolmogorov passage time, is higher than the rate implied by t_ν by a factor of $Re^{\frac{1}{4}}$. In the case that local concentration values are integrated over larger spatial or temporal intervals, the measured instantaneous value is smeared and not entirely representative of the true one. Furthermore, if the measuring probe is unable to resolve these high frequencies, the estimated variance and dissipation rate of the scalar fluctuations are lower than their true values.

For measurements over a large number of points in the flow field that are to be correlated in space and time, the above considerations may place a stringent requirement on the system throughput rate. In particular, if the sampling interval is t_ν and measurements over N spatial locations are to be performed, the sustained throughput rate must be of the order of $(NRe^{\frac{3}{4}})/T$. Therefore, the capabilities of the data acquisition system (presumably fixed) place an upper limit on the local values of Re and T that may be investigated at a certain resolution.

Radial LIF experiments were performed at the dimensionless axial distance of $x/d = 48.5$, 75, 105, and 150. In all cases, the image ratio and beam width combination resulted in a spatial resolution of the order of the local Kolmogorov scale. For each experiment, the Reynolds number and the axial distance from the flow source guided the selection of the array scanning rate and the data recording rate, so that optimal temporal resolution and sufficient record length were obtained. Thus, in all cases the line scan time was comparable with or less than the estimated Kolmogorov passage time, to ensure that the details of the concentration field were not smeared by the time integration inherent in the technique. The operating conditions for the

experimental runs are summarized in table 1 for jets and table 2 for plumes. In addition to the radial measurements, the concentration pattern in the axial direction as a function of time was also measured in a buoyant jet (1 cm nozzle) in the axial range from nozzle exit to $x/d = 118$. The initial value of the Richardson number was 0.20. A pure momentum jet of $Re = 5600$ at the same configuration was also recorded. For both cases 5120 individual axial profiles were obtained, using a line scan time of 11.2 ms, and a recording interval of 44.8 ms. The interpretation of these data will be presented in §4.6

3.2. *Radial profiles of concentration*

The instantaneous fluorescence profiles were converted to profiles of instantaneous tracer concentration by use of the method proposed by Koochesfahani (1984). An optical transfer function (incorporating the non-uniformities and imperfections of the imaging system, individual pixel response non-uniformity, etc.) is determined by measuring the array output at a known dye concentration before the experiment. Then, for each recorded scan, the effects of laser beam attenuation are removed in a recursive manner. The local fluorescence intensity is proportional to the local dye concentration and to the local beam intensity, which weakens in its traverse of the dye-containing region. The attenuation parameter was measured to be 0.005 cm^{-1} (10^{-7}) molar for the operating conditions of the experiments.

Typical examples of instantaneous concentration profiles across both jets and plumes, are presented in non-dimensional form in figure 4(*a–d*). It is apparent that these profiles bear no resemblance to the usual Gaussian profiles associated with mean (time-averaged) concentration distributions. There exist large local variations in concentration level resulting in steep gradients in the radial direction. High values of concentration occur in regions remote from the centreline of the flow. On the other hand, low-concentration fluid, or unmixed ambient fluid, may be found in regions close to the centreline. In comparison to the jet, ambient fluid is typically found in larger parcels in the plume interior. The detailed instantaneous plume profile (figure 4*d*) suggests that the concentration variations are more abrupt and occur over smaller spatial scales in the plume than in the jet (figure 4*c*). Another noteworthy feature of the plume flow is that the very high values of the concentration occur over spatially small scales, which are exhibited as very narrow spikes in these instantaneous profiles.

Ensemble averaging of only 25 such instantaneous concentration profiles did converge to the usual Gaussian profile but only if the ensemble consisted of profiles that were sufficiently separated in time. This ensemble size was also used by Uberoi & Singh (1975), who recorded instantaneous profiles in a plane jet that were uncorrelated in time. However, if the profiles in the ensemble are consecutive, a rough convergence to the mean profile shape is accomplished only if the number of profiles that are summed is enough to span one or two large-scale times of the flow (in the present case about 300 profiles). This characteristic serves to illustrate the underlying 'non-randomness' of the flow, as well as the relevance of the large-scale time.

The radial profiles of r.m.s. concentration fluctuation in a momentum jet and buoyant plume, normalized by the mean concentration value at the centreline, are presented in figure 5(*a*, *b*). The normalization used is intended to indicate the relative 'intensity' of turbulent concentration fluctuations. The fluctuation intensity measured by the probes is generally higher than that reported previously. There are two points that should be made here concerning this disagreement. First, since the

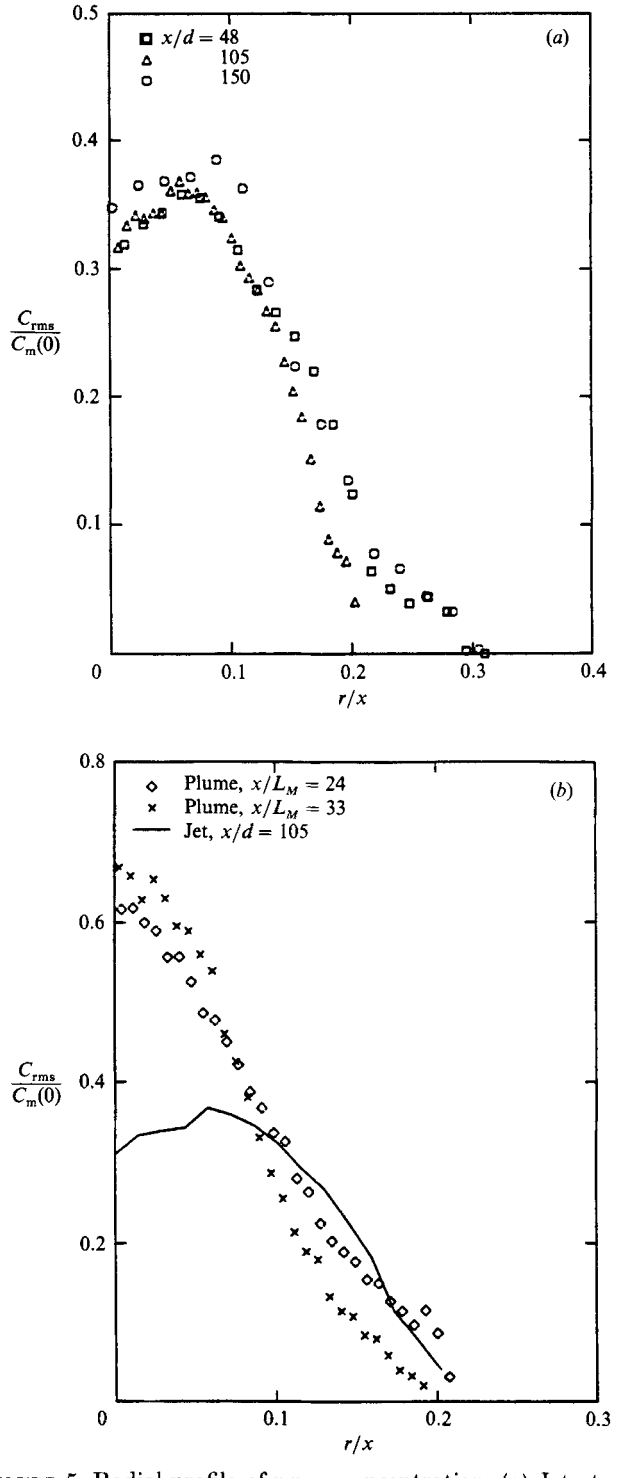

FIGURE 5. Radial profile of r.m.s. concentration. (*a*) Jet at x/d shown, (*b*) plume at x/L_M as shown.

Author	x/d	C_{rms}/C_m	Comments
Antonia *et al.* (1975)	59	0.22	heated air/air
Birch *et al.* (1978)	70	0.28	methane/air
Becker *et al.* (1967)	64	0.22	air/air
Corrsin & Uberoi (1950)	30	0.18	air/air
Dahm (1985)	300	0.30	water/water
Papanicolaou & List (1988)	98	0.22	water/water
Present results	150	0.34	water/water

TABLE 3. Fluctuation intensities in the momentum jet.

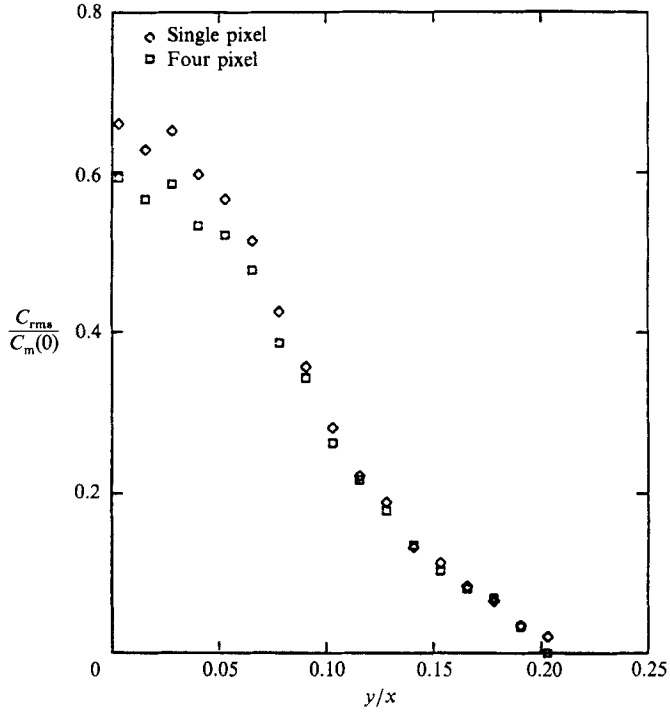

FIGURE 6. Effect of spatial resolution in computation of r.m.s. fluctuations in a plume.

concentration fluctuation intensity is due to interfaces (eddies) of all scales, it is reasonable to expect that the higher the probe resolution (both in space and time), the higher the value of concentration fluctuation intensity measured. The correct value is theoretically obtained in the limit by a probe that can resolve all flow scales, including the Batchelor scale. For the present measurements, the spatial probe resolution is relatively high compared to measurements with a wire probe that has inadequate response to large-amplitude fluctuations. Second, most reported values are for gas-phase jets, which have a Schmidt number of the order of unity, as compared with the present measurements at $Sc \approx 600$. It should be expected (Sawford & Hunt 1986) that molecular mixing (and the associated smoothing of concentration interfaces) is smaller at higher values of Sc. Representative values reported by previous investigators are rather scattered but such trends may be discerned from Table 3.

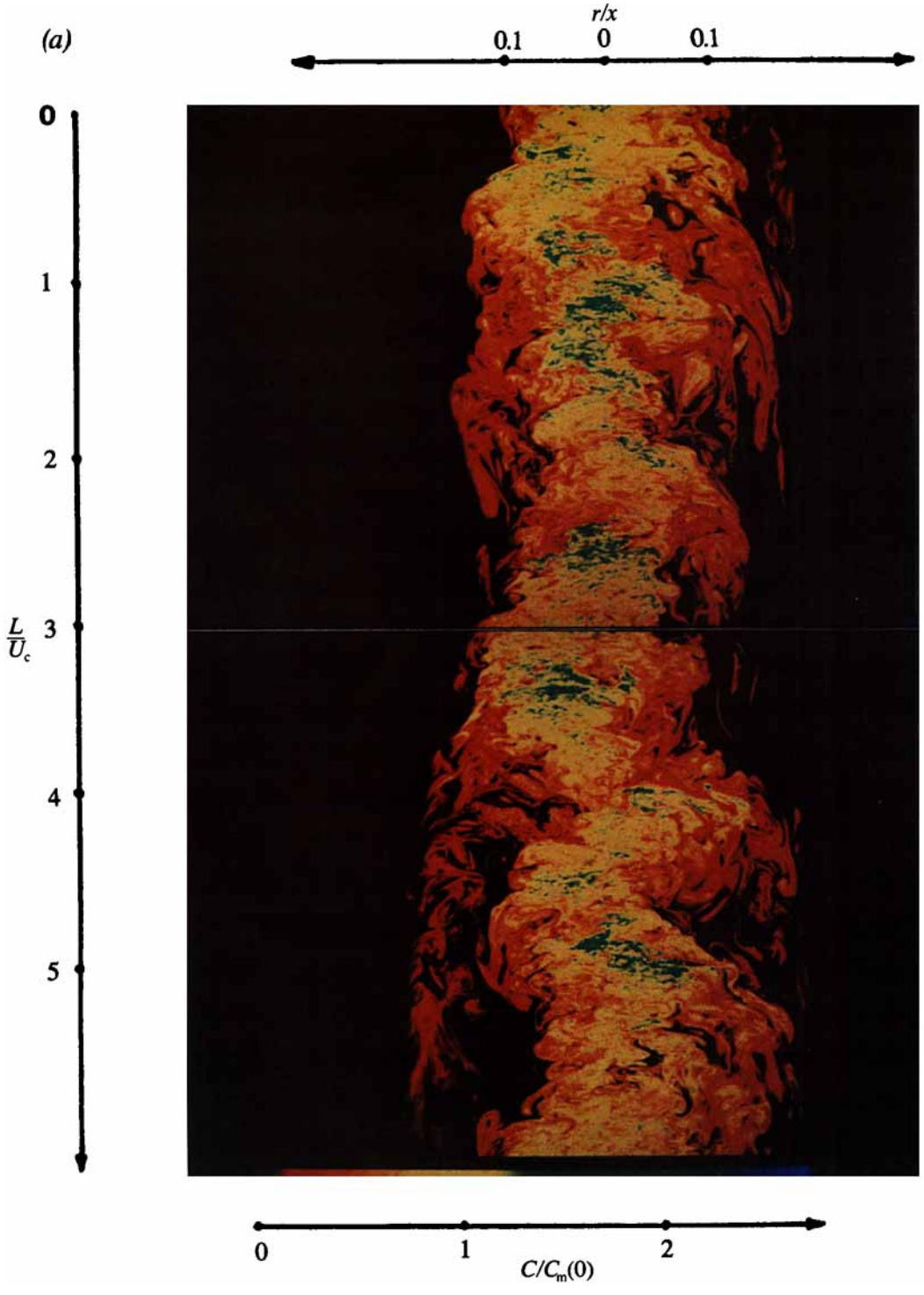

FIGURE 7*(a)*. For caption see facing page.

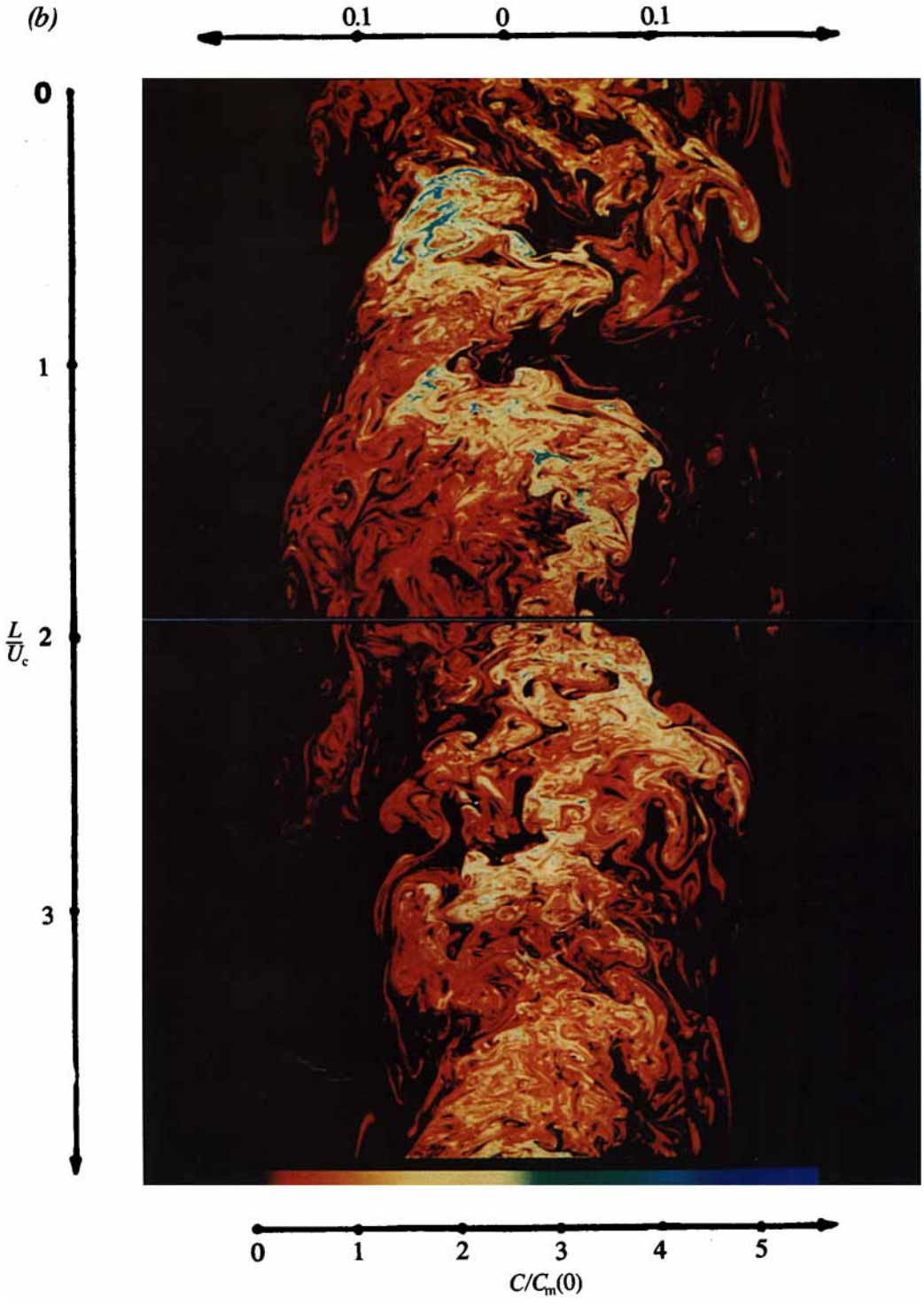

FIGURE 7. False colour image of time evolution of the instantaneous radial concentration profile. *(a)* Jet at Re=5600, x/d=150. *(b)* Plume at x/L_M=33, x/d=105.

FIGURE 8. Details of time evolution of the instantaneous radial concentration profile within a large structure in a jet at Re=9600, x/d=150. Total time 10.67 s.

For the buoyancy-driven plume, the normalized r.m.s. concentration profile shows that at the centre of the flow the magnitude of the fluctuation intensity is roughly twice that of the momentum-driven jet. The values measured are higher than the values measured previously by Papanicolaou & List (1988) and other investigators. Such high values indicate that the flow is very intermittent, which will be confirmed by the analysis presented subsequently.

To investigate how the probe resolution affects the results, the r.m.s. profile calculations were repeated at selected points within the layer using the spatially averaged values of four neighbouring pixels instead of the instantaneous pixel value. This procedure in effect approximately simulates the response of a probe with a decreased spatial resolution. The results for the plume flow are plotted in figure 6. As might be expected, an obvious trend of decreasing fluctuation intensity for decreasing spatial resolution is shown.

3.3. *Time evolution of the instantaneous profile*

An effective way of presenting the time evolution of the entire instantaneous concentration profile is to employ an image array processor equipped with a high-resolution monitor. Such a system (De Anza 6400) was extensively used in this investigation for the purpose of data analysis and display. To visualize the evolution of the patterns in the flow, a large number (up to 512) of concentration profiles are successively fed into the memory of the image array processor and displayed simultaneously as horizontal lines in the high-resolution video monitor (Conrac). Each scan line of the monitor depicts 512 individual pixels. When displaying data recorded at a density of 1024 pixels per Reticon camera array scan, one data pixel is skipped per one displayed. The display hardware has 8-bit colour depth, so that the 256-level range of the data is retained. By setting the intensity transformation tables in the image array processor appropriately, the red, green, and blue electron guns of the monitor are manipulated so as to assign different colours of varying intensity to different values of the concentration level. With this false-colour assignment the viewer is aided in identifying regions with uniform concentration since the eye is not accustomed to discerning monochrome variations of so many levels.

Pictures of the monitor, depicting the evolution of the instantaneous concentration profile at the axial distance of 150 nozzle diameters in the momentum jet, are presented in figures 7 (*a*) and 8 (plates 1 and 3). In figure 7 (*a*) the vertical axis is time, where the 960 successive profiles of $Re = 5600$ jet that are presented span approximately 39 s, equivalent to about 6 large-scale flow times. In figure 8 details of a structure within a jet at $Re = 9000$ are shown. The large-scale time in this case is approximately 8.2 s and the complete picture represents 5.36 s of record. The digital data displayed in these figures reveal some important features of the instantaneous concentration field in the fully developed jet flow. It is clear that, despite the random characteristics typical of the turbulent flow, there is a certain regularity manifested by the passage of large structures at time intervals roughly equal to T_j. The front of such a structure is marked by a spatially coherent increase in concentration level relative to that of the preceding (in time) fluid. The central region of the flow is usually at a higher concentration than the side regions, where pockets of ambient fluid are frequently found. High-concentration regions are observed to sway at positions off the jet centreline. This may be suggestive of a helical structure in the main flow which, owing to the limitations inherent to the present technique, cannot be verified.

Such features are also observable in the spatially and temporally resolved still

photographs in figures 1–3. However, the digital data presented here permit a more precise statement to be made regarding the uniformity in fluid concentration at any instant as it passes through the measuring station. The colour assignment aids the identification of three (crudely defined) levels of concentration. Fluid at the lowest concentration level marked by shades of red colour (black means no dye) is usually found at regions away from the centreline as well as the back (upstream) regions of the large structures. The elongated contours in the time direction, indicate that at large radial distances fluid is relatively stagnant. This is generally consistent with the observations of Shlien (1987). Fluid parcels that are ejected radially outwards will stagnate for some time (maybe during the passage of a large scale or more) before they will become re-entrained into the jet. Fluid at the mid-concentration level is typically found around the central region of the instantaneous profile, which is not fixed in space. This is marked by yellow colour. The transition from red to yellow is not always smooth, indicating a step in the concentration value. Finally, regions of highest concentration, that are marked by shades of green and occasionally green–blue colour, are most frequently found at the front (downstream) regions of the large structures. Since at the back of the structure the concentration level is rather low, and marked by the occasional presence of clear ambient fluid, the transition in local concentration level at the instance of the arrival of a large structure can be very sharp, indicating a steep local gradient.

The classification of the fluid states as belonging to three levels of concentration is rather arbitrary. In fact, there is a subjective aspect in this classification since there are variations of concentration level (and correspondingly of colour shade and intensity) inside each colour band that the photographic film may or may not pick up. However, this classification aids in the identification of separate regions of widely varying levels of intensity. The inclusion of the blue colour in the presentation of the data is intended to highlight the highest concentration values and the steep gradients that characterize the structure fronts. Our attempts to quantify these observations are presented along with a discussion on the shape and representative features of the large structure.

A similar image of digital data from the colour monitor for a buoyant plume flow is presented in figure 7 (*b*) (plate 2). The vertical (time) axis also spans 960 individual array scans, corresponding in this case to about 4 large-scale times. These data were taken at an axial distance of 105 diameters from the plume source, corresponding to $x/L_M = 33$. As before, only one of every two available data pixels is actually displayed on the monitor.

It can be observed that a change in the instantaneous flow structure occurs under the action of buoyancy. In contrast to the jet flow, it is no longer possible to identify a central 'column' where concentration values are relatively uniform. The flow is very intermittent; the probability of finding unmixed ambient fluid is substantial everywhere in the interior of the plume. Even where ambient fluid is absent, local fluctuations of concentration intensity are strong (marked by the intertwining of yellow ribbon-like patches in a red background). It is also evident that local concentrations occasionally reach very high levels compared with the local mean value or even the maximum mean value. These are marked by the presence of small regions of green–blue colour. It should be noted that these are roughly three to four times the mean centreline concentration level. It is still possible, as in the jet, to identify concentration structures that convect past the measuring station at time intervals given roughly by the large-scale time. Based on observations of longer time records it was concluded that, as in the jet and perhaps even more so, fluid at the

highest *concentration* is found in the regions identifiable as the large-structure 'fronts'. In the buoyant flow there is a direct connection between local dye concentration level and local density difference (or buoyancy force). As a consequence, regions marked with high values of dye concentration are expected to be moving faster than surrounding parcels of low dye concentration. This is consistent with the notion that the front region of the structure is its most undiluted part and it would also imply that different parts of the large structure convect at different speeds.

Another difference between the entrainment mechanism of the jet and the plume is that fluid at the boundaries of the buoyant flow does not tend to stagnate awaiting re-entrainment. In fact, observation of the shapes of smaller structures at the plume boundaries indicates that they are overturning and thus actively entraining ambient fluid. The long vertical streaks often present at large radial distances in the momentum jet flow are notably absent in the plume. In comparison with the jet, eddies of a greater variety of scales and at different positions seem capable of entraining. This is consistent with the greater dilution capability of the buoyancy-driven flow compared to the momentum-driven flow.

4. Turbulent structure of concentration field

The flow visualization results are suggestive of a flow that has some order imposed on an apparently random background. As in any random process, neither its time evolution can be predicted by a deterministic function, nor can the value at a particular time be predicted by an ensemble of realizations. Statistical methods are therefore appropriate for an analysis of such signals and have been widely used to characterize various turbulent flow quantities. In what follows, we present a sampling of the results of such methods to the dilution data obtained by the LIF method.

4.1. *Intermittency and conditional averaging*

To quantify the extent of the presence of unmixed fluid at various radial positions in the flow field and determine the shape of the mean 'mixed' profile, the following scheme was adopted. First, a subsidiary time-dependent intermittency variable with a value of 0 or 1 is assigned to the instantaneous concentration C at a point according to whether C exceeds a certain threshold. The intermittency at that point then follows from the conventional time average of this intermittency variable. A time-averaged mean mixed profile of concentration can also be developed from a conditional average of the concentration at a point in the usual way by averaging the product of the concentration and intermittency variable. It was found that the shape of the mean mixed profile and the intermittency profile were not sensitive to the value of the threshold in the range of 5% to 15% of the mean centreline value. The threshold value for all radial positions was arbitrarily chosen to be 10% of the mean centreline value at the axial location of the experiment.

The radial intermittency profile in the far field of a momentum jet is shown in figure 9. It may be seen that, from a statistical point of view, not much ambient fluid reaches the jet centreline. Of course the technique employed here only permits identification of unmixed fluid down to the scale that can be resolved. It is obvious that sharp interfaces between unmixed fluid and dye containing fluid at scales smaller than the resolution limit will appear mixed to the probe. So in that sense, our intermittency estimate should be viewed as an upper limit of the true value obtained

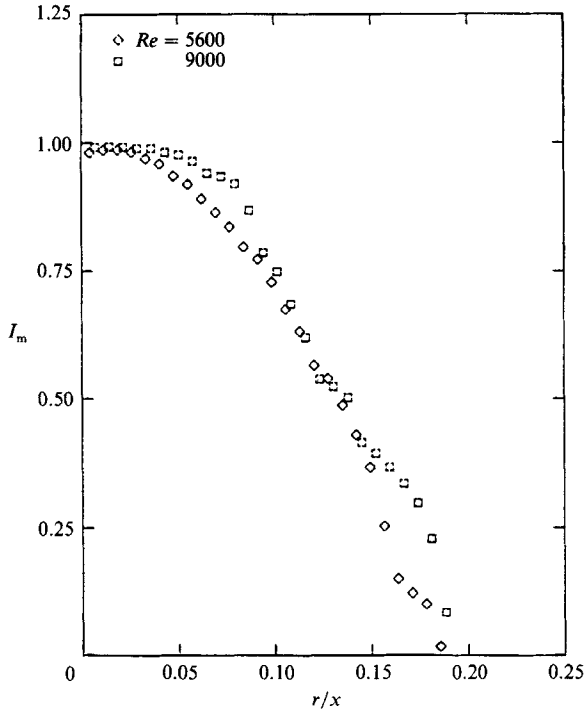

FIGURE 9. Radial profile of intermittency in a jet, at $x/d = 105$.

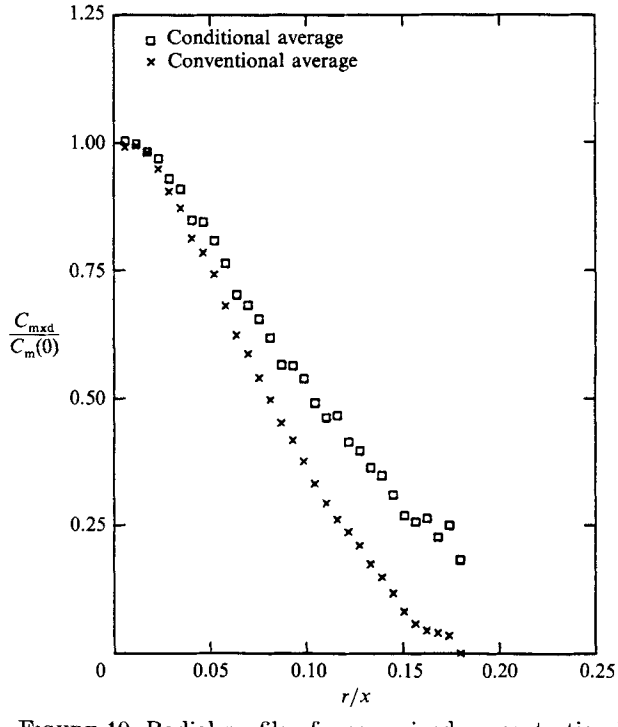

FIGURE 10. Radial profile of mean mixed concentration in a jet.

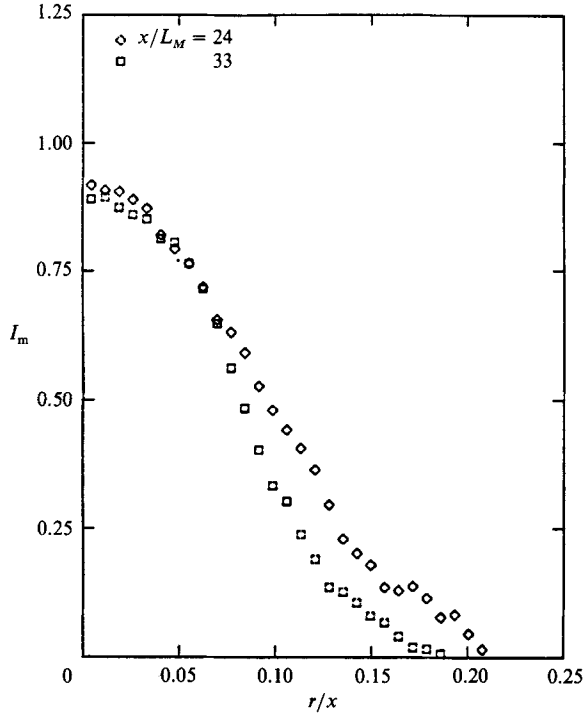

FIGURE 11. Radial profile of intermittency in a plume.

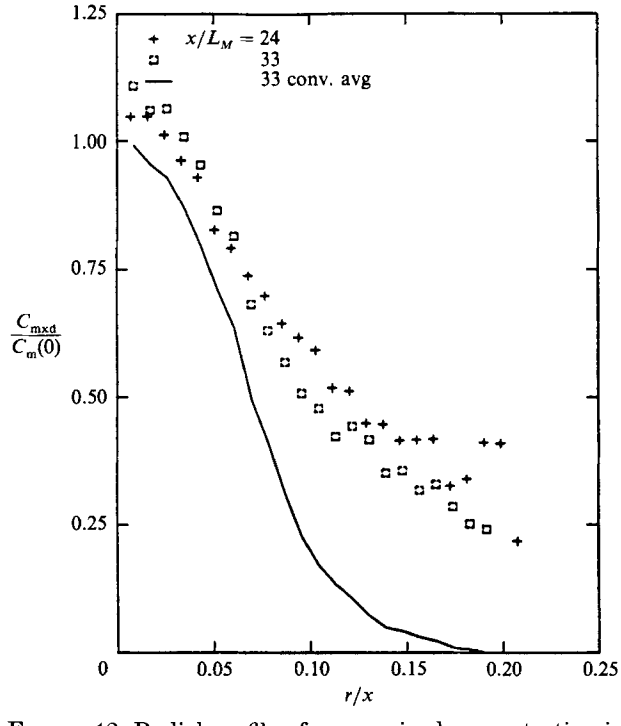

FIGURE 12. Radial profile of mean mixed concentration in a plume.

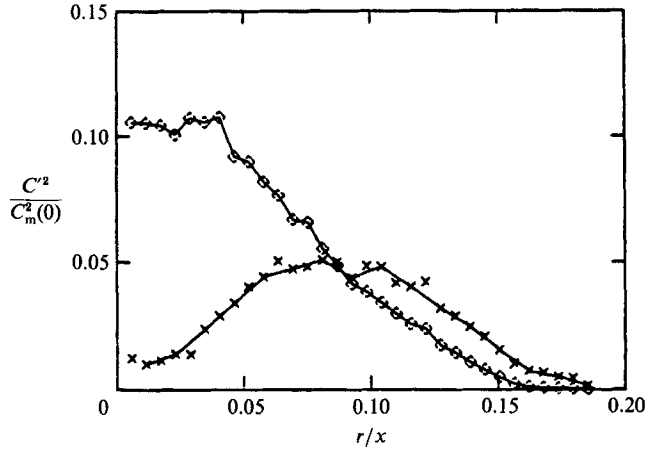

FIGURE 13. Radial profile of contribution to concentration variance from unmixed (×) and mixed (◇) fluid in a jet.

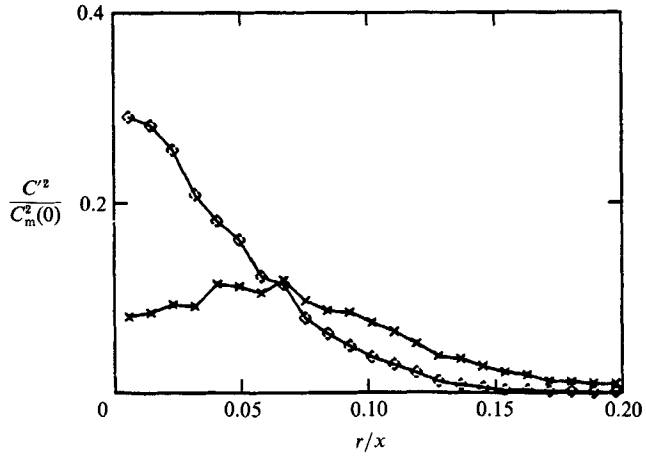

FIGURE 14. Radial profile of contribution to concentration variance from unmixed (×) and mixed (◇) fluid in a plume.

from an ideal probe that can resolve all scales. The mean mixed concentration profile in the momentum jet is shown in figure 10. In comparison with the conventionally averaged profile it is much fuller, reflecting the presence of high-concentration fluid at radial positions off the centreline. In a way, it is more representative of the instantaneous concentration profile; however, the sharp local gradients of the instantaneous profiles are still smoothed out by the averaging procedure, and no central 'column' of relatively uniform concentration may be discerned.

The intermittency profile and mean mixed profile for the buoyant plume are shown in figures 11 and 12. It is clear that a substantial amount of very low-concentration fluid or clear ambient fluid can be found in the plume interior. The mixed profile in the plume is also fuller than the conventionally averaged profile. It is implied that high concentrations are also common at positions off the centreline under buoyant conditions.

A similar conditional-averaging procedure can be applied to the concentration

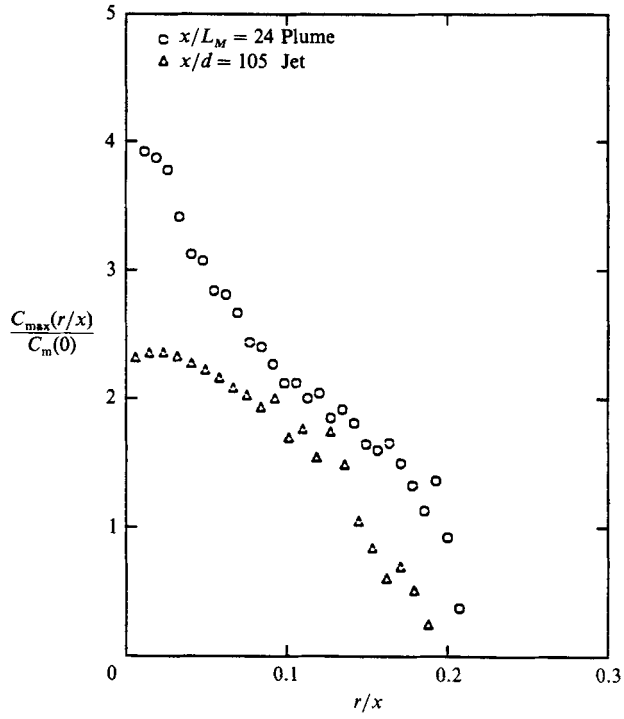

FIGURE 15. Maximum normalized concentration as a function of radial position in a jet and plume.

variance. The purpose in this case is to estimate the contribution to the computed turbulence intensity from the presence of ambient fluid in the flow interior. The results are plotted in figures 13 and 14. The contribution of unmixed fluid to the variance (C_{rmsc}) is overall more important in the buoyant flow and has an off centreline peak at $\eta = r/x = 0.075$. (The value of the peak clearly depends on the value of the threshold chosen, but the qualitative effect is the same). There is a notable similarity between the turbulent structure of the momentum jet and the buoyant plume, as evidenced from these figures. A similar behaviour was exhibited in the plane buoyant flow geometry investigated by Kotsovinos (1977).

4.2. *Radial profile of maximum concentration*

The maximum concentration C_{max}, measured during the sampling time and non-dimensionalized by the mean centreline concentration, is plotted in figure 15. The profile of minimum concentration is not plotted since it was zero throughout the radial extent of the flow. The radial boundary of the flow can be defined as the distance r/x at which the profile of maximum recorded concentration drops abruptly to zero. It is evident that the dimensionless maximum and minimum concentration depends strongly on the presence of buoyancy. This is also the case for the plane plume (Kotsovinos 1977). The greater spread in local concentration level is reflected in the higher values of r.m.s. turbulence intensity observed in the buoyant flow. It can also be observed that high concentration values (in excess of the mean centreline value are recorded at large radial distances.

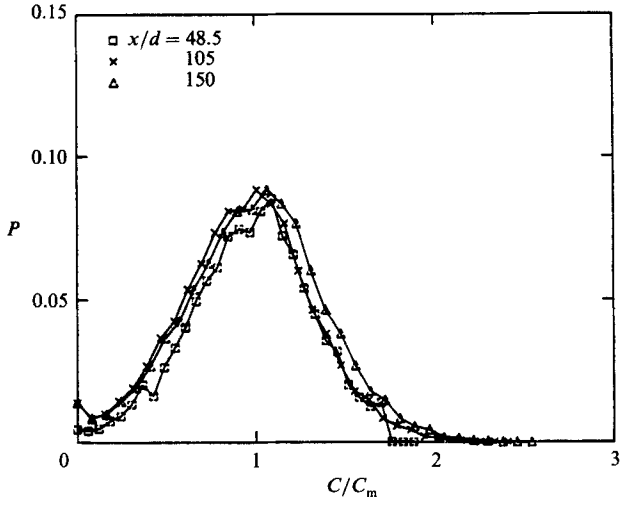

FIGURE 16. Probability density function of normalized concentration at jet centreline as a function of dimensionless axial distance.

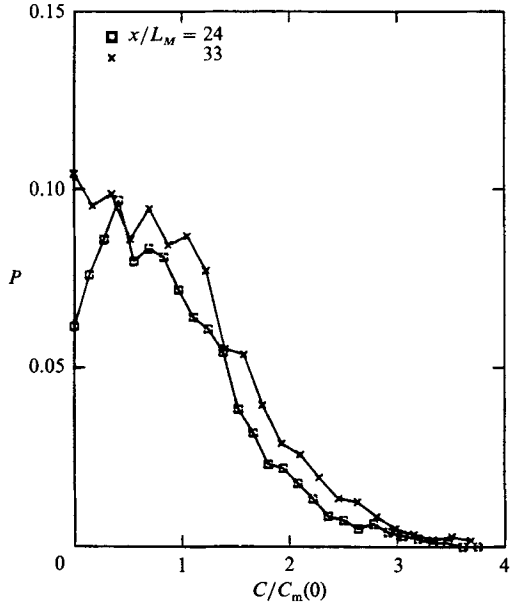

FIGURE 17. Probability density function of normalized concentration at plume centreline as a function of dimensionless axial distance.

4.3. *Probability density function for concentration*

The probability density function (p.d.f.) of dimensionless concentration was determined for various radial positions in the flow. The p.d.f. is normalized by the requirement that its integral is unity. The shape of the concentration p.d.f. is of interest in cases where a statistical approach is taken in problems involving the prediction of transport, mixing, and chemical reactions in turbulent shear flows (Toor 1962; Pope 1981; Effelsberg & Peters 1983). The p.d.f. yields a more complete

representation of a random variable than the mean and r.m.s. values, which are obtainable from the first and second moments of the p.d.f. respectively.

For the computation of the p.d.f., each instantaneous concentration value C was divided by the local average centreline value C_m. The p.d.f. of the normalized concentration variable C/C_m at the centreline of the momentum jet flow is presented in figure 16 for various values of the non-dimensional axial distance from the source. From this representation, it may be observed that the p.d.f. shape exhibits similarity with axial distance, which is required on dimensional grounds. The p.d.f. is rather symmetric at the centreline, with some preference for lower values (skewness).

The p.d.f. of normalized concentration at the centreline of the buoyant plume is presented in figure 17. It may be seen that, contrary to what occurs for the momentum jet flow, the most probable value is not the mean value, owing to the high probability of detecting fluid of small or zero concentration. The intermittency, as defined above, was confirmed to increase for an increased value of the dimensionless distance x/L_M. This behaviour raises the question of how the flow would behave at even higher values of x/L_M or, equivalently, whether 'fully buoyant' conditions have been realized. However, accurate study of buoyant jet flows at higher values of x/L_M than obtained here was operationally very difficult in our facility and this question must be resolved by other means.

4.4. *Integral scale of concentration fluctuations*

In this section, some results are presented that are obtained from a correlation analysis of the concentration data. These include correlation functions and estimates of the integral scale of concentration fluctuations.

The autocorrelation function of the concentration time signal at a fixed point in space is computed as

$$R(\tau) = \overline{c(\eta, t)\, c(\eta, t+\tau)},$$

where τ is a variable time delay and $c(\eta, t) = C(\eta, t) - C_m(\eta)$. The cross-correlation function between time signals at two points in space is computed in a similar manner as

$$R(\tau) = \overline{c(\eta_1, t)\, c(\eta_2, t+\tau)}.$$

Unbiased estimates of these quantities ('unbiased' refers to the method of time averaging) were computed directly from concentration time series for selected points in the flow field. These are presented in figure 18 for the momentum jet and figure 19 for the buoyant plume, as a function of the normalized time delay. All the functions are normalized with their value at zero time delay. It is observed that the large-scale periodicity of the data shows up as a secondary peak for large enough values of the time delay. This peak is always more pronounced in the cross-correlation function. The general shape of the cross-correlation functions resembles that of a sine wave in broadband noise. It is surprising that this large-scale frequency was not discerned in previously measured correlation functions reported in the literature. It is possible that previous investigators did not extend the computation of the correlation function for sufficient time delay. It is also possible that, owing to the wandering of the entire jet column simultaneous sampling with two probes that are separated by a small distance is actually necessary for the identification of the large-scale passage frequency through the cross-correlation.

In comparison to the jet, the secondary peak corresponding to the large-scale passage frequency is not as pronounced in the plume autocorrelation functions,

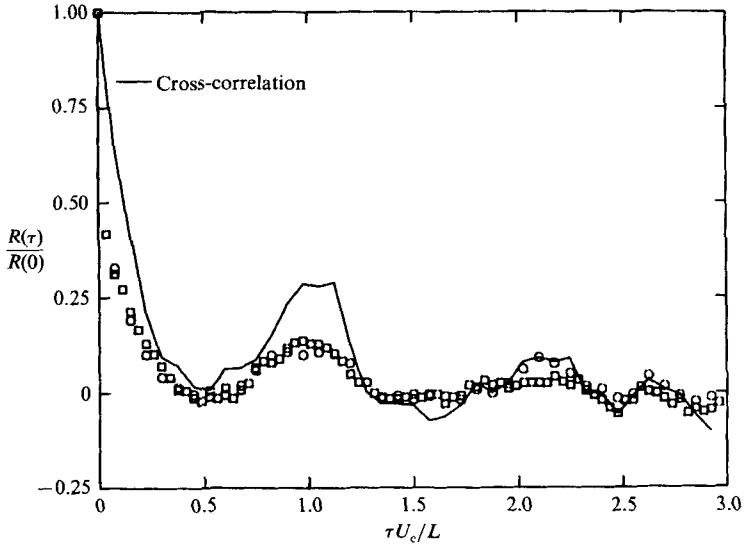

FIGURE 18. Normalized correlation functions with variable time delay in a jet.

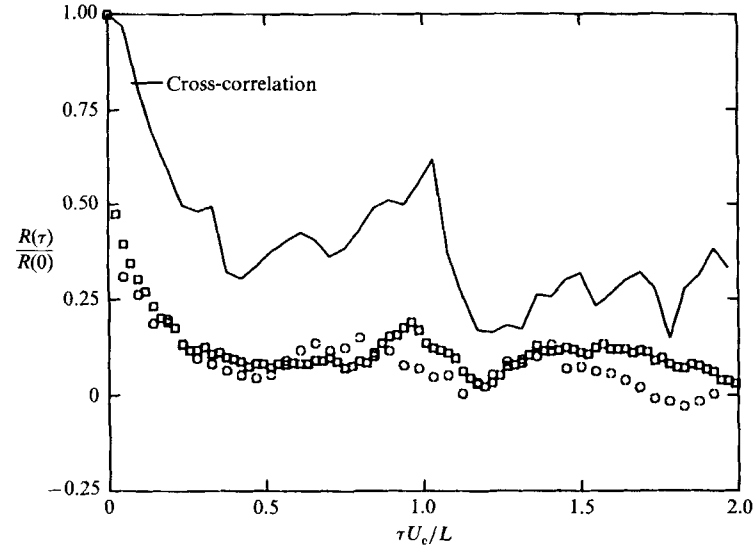

FIGURE 19. Normalized correlation functions with variable time delay in a plume. □, Auto, $r/x = 0$; ○, auto $r/x = 0.01$.

possibly owing to the increased wandering of the structures in fixed physical coordinates. However, the peak in the cross-correlation functions is even more pronounced. The good agreement of the autocorrelation functions for small time delay in the momentum and buoyant flows presented in figure 20 shows that the details of the small-scale flow structure in the axial direction are independent of the large-scale configuration. However, as will be shown shortly, this is not the case for the spatial correlations in the radial direction.

A correlation function that can also be computed from the data is the lateral spatial correlation for zero time delay defined as

$$R(\xi) = \overline{c(r,t)\,c(r+\xi,t)}.$$

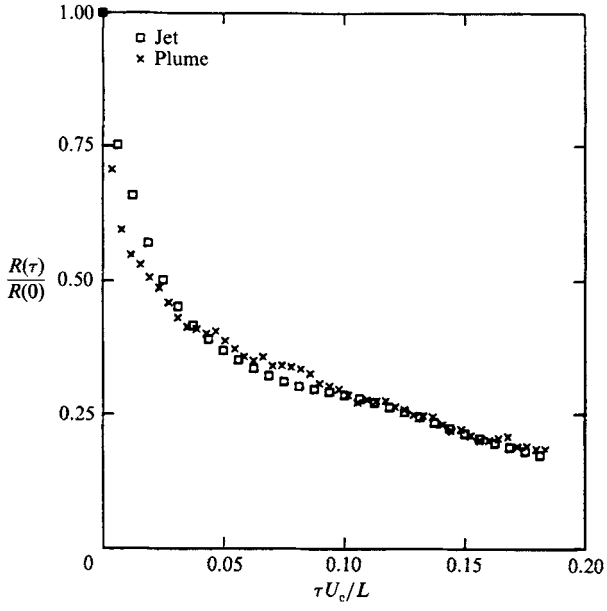

FIGURE 20. Normalized autocorrelation function for small time delay at centreline for both a jet and plume. □ Auto, $r/x = 0$; ○, auto $r/x = 0.002$.

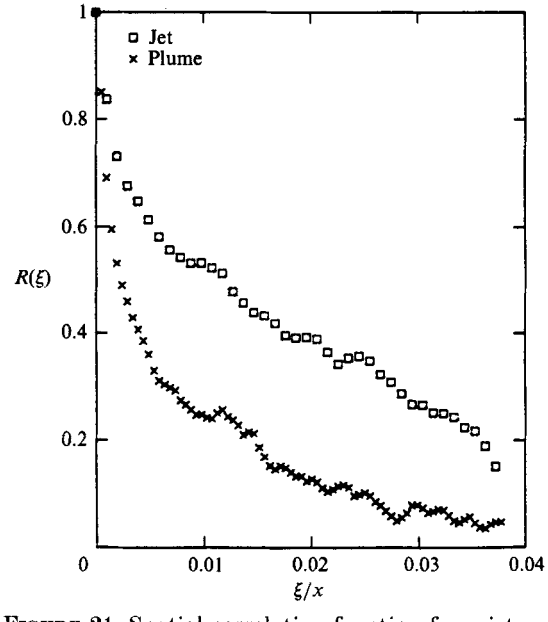

FIGURE 21. Spatial correlation function for a jet and plume.

This estimate does not invoke Taylor's 'frozen turbulence' hypothesis, as it is directly computed over spatial increments. Representative estimates of this function, computed at the flow centreline at the axial station of $x/d = 105$, are presented in figure 21. As before, normalization with the value at zero separation is used. Note that the nature of the data acquisition method, i.e. sequential sampling of adjacent points in space, will inevitably degrade the estimates of the spatial correlation

Jet					Plume				
Re	x/d	r/x	Λ/x	TU_m/x	x/L_M	x/d	r/x	Λ/x	TU_m/x
5600	150	0	0.041	0.032	24	105	0	0.018	0.096
5600	150	0.1	0.046	0.123	24	105	0.02	0.018	0.071
5600	105	0	0.029	0.034	24	105	0.044	0.022	—
9000	105	0	0.026	0.162	33	105	0	0.011	0.022

TABLE 4. Integral scales of concentration fluctuations.

function at very large values of ξ. However, since in the worst case the time lapse between sampling at the largest separation shown is only 0.8 ms and the local convection velocity is less than about 3 cm/s, it is believed that insignificant error is introduced in the estimates of the spatial correlation function for the values of separation presented here. The shape of this function indicates in a direct manner the extent of correlation of the concentration fluctuations in physical space in the radial direction. Geometrical considerations imply that it should be an even function of ξ (Hinze 1975). For small values of ξ it was confirmed that it is indeed so for any point in the flow field. However, an asymmetry is inevitably introduced for large ξ when the centre point is at locations off the flow centreline. This is due to the obvious lack of homogeneity of the flow.

A comparison of the shape of the spatial correlation functions confirms that the presence of buoyancy generally acts to decrease the extent of correlation in physical space in a direction normal to gravity. This is intimately related to the strongly intermittent character of the buoyant flow. The disagreement of the spatial correlation functions in the lateral direction for both the momentum and buoyant flow indicates that buoyancy affects the small eddy structure preferentially in the lateral direction. This result is consistent with earlier qualitative observations, where it was noted that the intertwining interfaces of the apparent vortical structures with axes in the flow direction are thinner in the plume flow and are marked with fluid of high concentration.

The integral timescale of concentration fluctuations is defined through the integral

$$T = \int_0^\infty R(\tau)\,\mathrm{d}\tau.$$

The lateral integral spatial scale is also defined by the corresponding relation

$$\Lambda = \int_0^\infty R(\xi)\,\mathrm{d}\xi.$$

Estimates of these integral scales (where the integral is taken over the positive portion of the correlation function) are presented in table 4. These results indicate that the integral lengthscale of the turbulence Λ is about 10% of the large scale L, and support the hypothesis that the integral scale is primarily responsible for the mixing in such flows.

4.5. *Large-scale features of the concentration pattern*

The photographs presented in figures 1–3 and the digital images of the type shown in figures 7 and 8 suggest that the dimension of the large structure is comparable with

the local flow width, and that it convects with the local convection velocity. Sreenivasan *et al.* (1979) analysed thoroughly the temperature and velocity time traces in a slightly heated turbulent air jet. Based on an ensemble-averaging procedure they found that ramp-like structures in the temperature (tracer) signal, whose time extent was comparable with the large-scale time of the flow, were statistically significant, and caused a breakdown of local isotropy. It is natural to associate these large-scale patterns with the signature of the large-scale structure observed in the far-field jet flow. Furthermore, a comparison between gas-phase and liquid-phase jets is of interest, because of the anticipated effects of the Schmidt number in the molecular mixing process.

For these reasons, a conceptually similar analysis of the concentration time traces was undertaken for the flows considered here. The concentration time signal was processed by the ensemble-averaging technique of Sreenivasan *et al.* which is outlined here. First, the duration (time interval) between two successive instants at which the signal exceeds, during an upcrossing, and falls below, during the subsequent downcrossing, a preset threshold is determined. If the duration lies within the range of interest, the amplitude level of the signal is obtained, by interpolation if necessary, at S equally spaced points within the excursion. (For convenience, S is chosen as the ratio of the mean duration over the sampling interval.) A subsequent excursion in the same range of duration is treated similarly, and the amplitudes at the S points are added to the previous set of values at the corresponding locations. The ensemble average, denoted by $\langle\ \rangle$, is obtained by dividing the sum at each of the S points by the total number N of excursions belonging to the chosen range of duration. For convenience, the expression 'duration T', is used to signify 'range of duration centred about $\bar{T}$', *where* $\bar{T}$ denotes the arithmetic mean of the extreme values of the chosen range. The interval $\Delta\bar{T}$ used for selecting members of the ensemble was $0.2\bar{T}$. Concentration traces corresponding to several neighbouring points were used to form each ensemble average. This not only improved the convergence of the ensemble shape, but also made the computed ensemble average more representative of the average concentration pattern in the large structure. For the purpose of the present analysis, two different probability density functions were also obtained for the ensemble. One p.d.f. was computed for the concentration values occurring for the leading half of the ensemble shape, and the second p.d.f. for the trailing half.

Representative ensemble shapes as computed by this procedure are presented in figures 22(*a*) and 23(*a*). Normalization is performed with the conventionally time-averaged concentration value at the same radial location in the layer. It should be noted that for small values of the normalized duration, the ensemble-average shape is symmetrical, whereas for durations comparable with the large-scale time an asymmetry is introduced. The effect of using a large number of neighbouring points (middle curve) for the ensemble is to smooth the ensemble shape and slightly reduce the front to back gradient. The resulting large-structure shape exhibits the characteristics that are observed in the digital display images such as figure 7(*a*, *b*). The concentration value is thus observed to rise in an abrupt manner in the (downstream) front, while it slopes more gradually in the (upstream) back regions. These results are in qualitative agreement with the structures observed by Sreenivasan *et al.* in the gas-phase coflowing jet. A quantitative difference is that in the present case, the average concentration gradient in the structure is generally smaller. Since part of the ensemble-averaged structure shape results from the increased (intermittent) presence of low-concentration fluid in the back regions, the two separate p.d.f.'s are also presented in figures 22(*b*) and 23(*b*) for a clarification

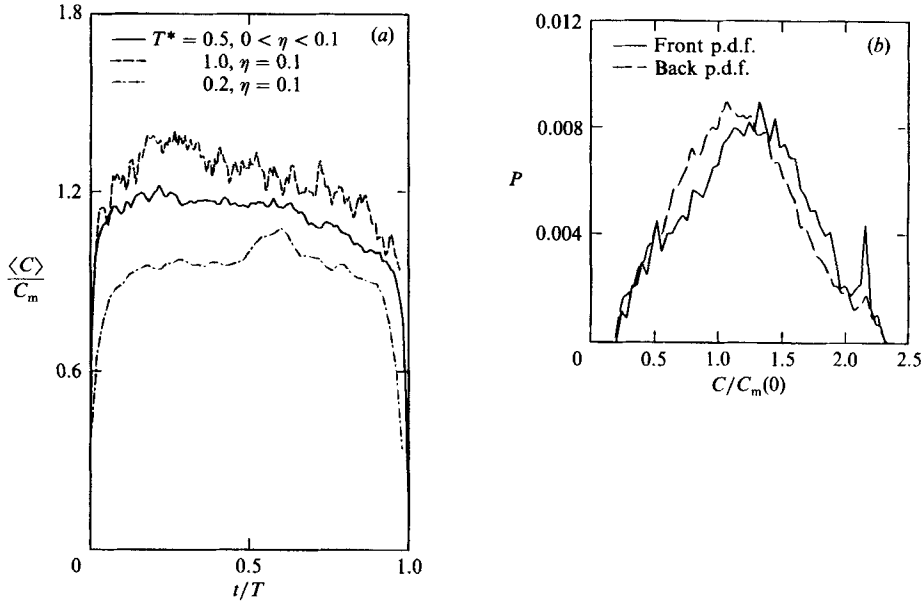

FIGURE 22. (*a*) Ensemble-average distributions of excursions in the normalized concentration signal in a jet. (*b*) P.d.f. of concentration in front and back regions of large-scale jet structure.

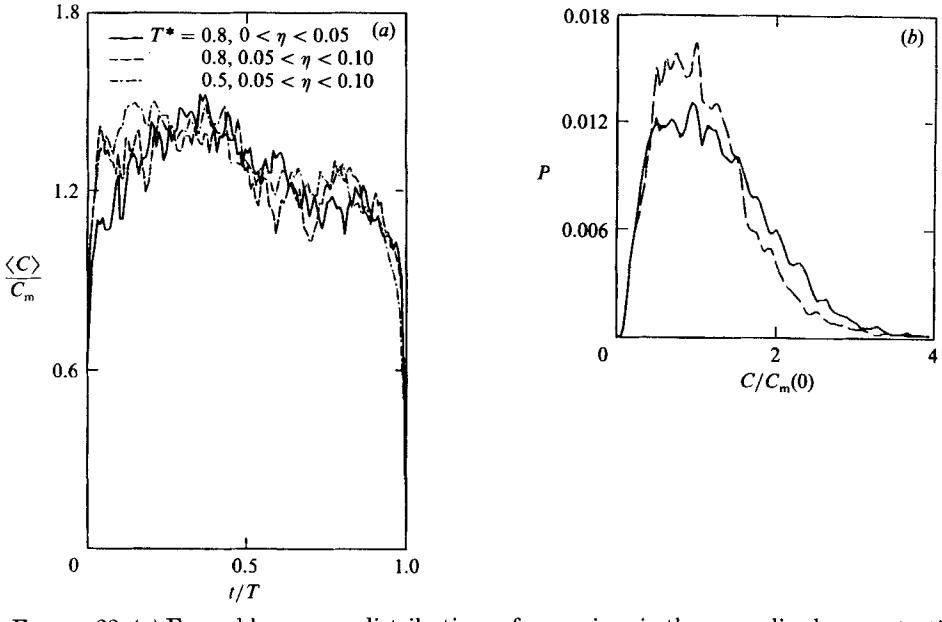

FIGURE 23. (*a*) Ensemble average distributions of excursions in the normalized concentration signal in a plume. (*b*) P.d.f. of concentration in front and back regions of large-scale plume structure.

of this issue. These correspond to the case of averaging over a large number of neighbouring pixels (middle curve of figure 22*a*) where some smoothing occurs. It is observed that the front-region p.d.f. is generally shifted with respect to higher values than the back-region p.d.f. This establishes that in the front region of the large structures there is a higher probability for the occurrence of high concentration fluid.

4.6. *Axial profiles of concentration and convection velocities*

The fluorescence profiles taken along the flow axis were converted to concentration profiles according to the procedure outlined in §3.2 and are presented in digital image format in figure 24(*a*, *b*). For this presentation instantaneous values of concentration have been divided by the local time-averaged values. A high value of the intensity thus corresponds to an unusually high value of the instantaneous concentration for the particular axial location; black corresponds to clear ambient fluid. The vertical axis is time and the 960 longitudinal concentration profiles, displayed as horizontal lines in these figures, span 42.7 s on the time axis. The entire axial range of flow is shown on the horizontal axis by skipping one pixel per one displayed. The strongly intermittent character of the plume flow (figure 24*b*) for a large part of the imaged axial range is noteworthy. It is also of interest that, confirming the earlier observations in jets by Dimotakis *et al.* (1983), the scaling required on dimensional grounds, $t \sim x^2$ for the momentum-driven flow (figure 24*a*), and $t \sim x^{\frac{4}{3}}$ for the buoyancy-driven flow, is obeyed only in an average sense for a particular concentration pattern. Most t–x patterns are somewhat piecewise linear. However, parabolic shapes for the overall t–x patterns are obtained in the jet flow by the connection of such piecewise linear segments. Groups of segments having an apparent common slope may be considered as belonging to a single 'structure'. The size of individual linear segments scales with axial distance, as required by similarity. A visual estimate is that the size of most such segments is about one local jet diameter ($0.4x$). The axial extent of the groups also scales in the same manner, suggesting that convection velocities are constant within each individual large structure. The variations in slope observed at a particular axial location as a function of time show how the convection velocity may vary from structure to structure. Segments with different slopes meet when a faster upstream structure 'rear ends' a slower one downstream. This is not the case for the plume, where structures do not seem to 'interact' in this manner. The front segments of large structures, in accordance with the results obtained from the radial measurements, are observed to be at a high concentration relative to the rest of the structure segments. Often, the high value (in a relative sense) at the structure front persists for a local lengthscale of the order of the local jet diameter. The high concentration values at fronts are more pronounced in plumes than in jets and they persist for a greater distance.

These t–x digital concentration data were used to evaluate the evolution of the axial convection velocity as a function of the distance from the flow source. For each axial location x_0, a correlation function $R(x_0, \xi)$ was evaluated by the following procedure. At each time instant t_i in the record, the concentration pattern in a neighbourhood of x_0 was first obtained by cubic spline interpolation over a number M of adjacent points. This step was repeated for the next time instant $t_i + \Delta t$ in the record (here $\Delta t = 0.04448$ s). The function $R(x_0, \xi; t_i)$ was then formed by summing the products $C(x_0+m, t_i)\,C(x_0+m+\xi, t_i+\Delta t)$ over the index $m = 1, M$ (the index defining the interpolated range). The procedure was repeated for all 5120 scans in the data set, and $R(x_0, \xi)$ was obtained by averaging over time. For each axial location considered, the correlation function so obtained is a smooth function of ξ, with a single maximum. The average convection velocity at the location x_0 was then obtained from the position $\xi_{\max}$ of the maximum of each correlation function by $U_c = \xi_{\max}/\Delta t$. These data are plotted as a function of the axial distance in figure 25, along with the direct measurements of the mean centreline velocity data for jets and plumes taken in our facility by Papanicolaou & List (1988). The results agree

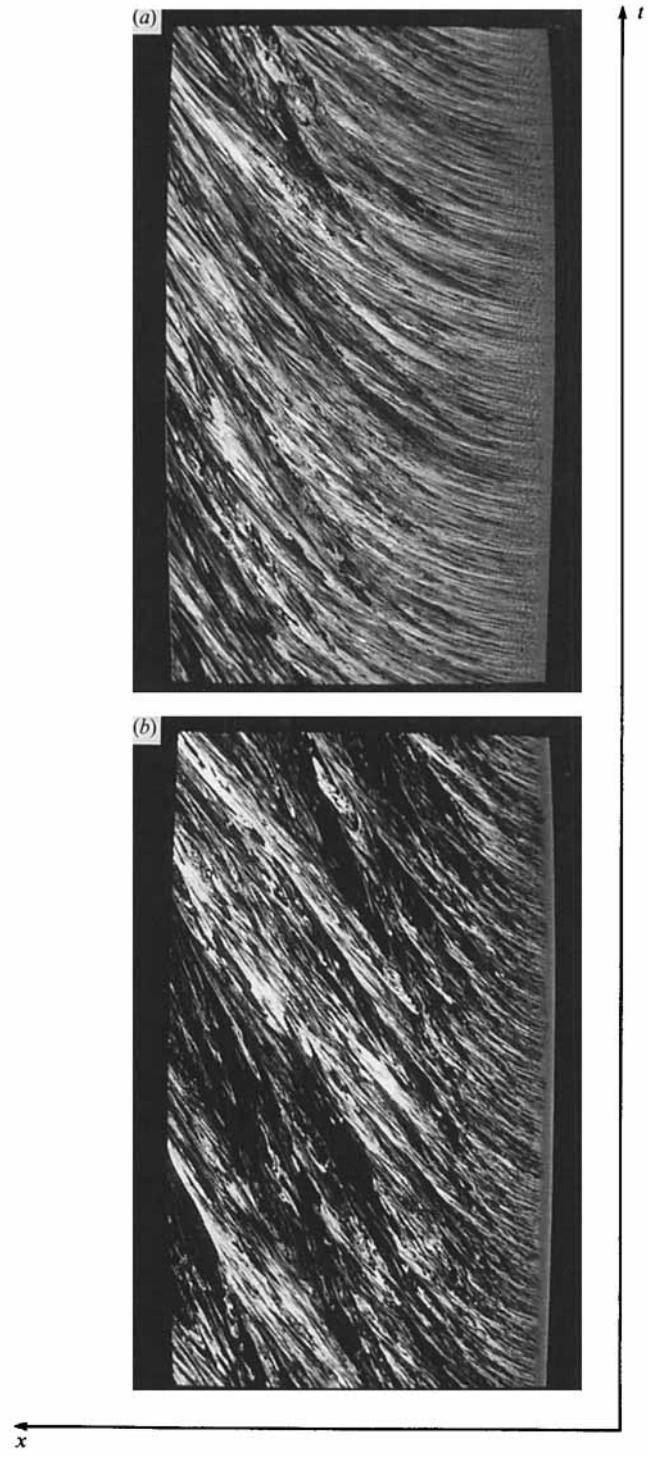

FIGURE 24. A time sequence of 960 concentration profiles along the axis of jets and plumes showing the t–x trajectories of structures; (*a*) jet, (*b*) plume.

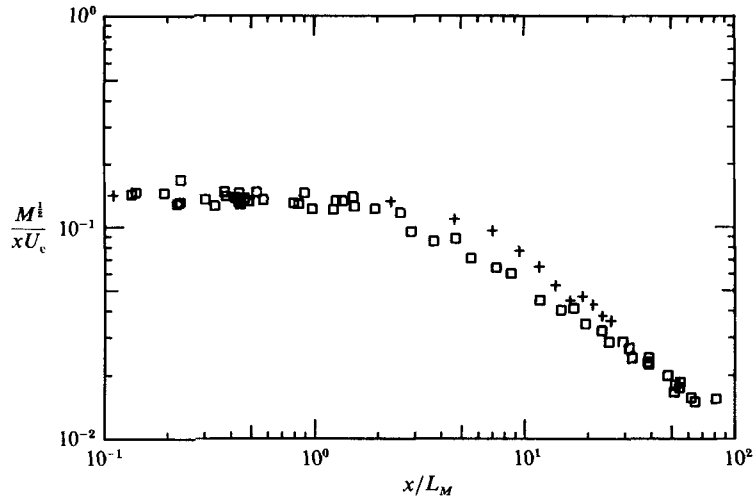

FIGURE 25. Convection velocities on the axis of jets and plumes derived from data in figure 24(*a*, *b*) by correlation analysis (+) plotted with data from Papanicolaou & List (1988)(□).

remarkably well for jets, where the data point shown is the mean of 10 realizations of the convection velocity. For plumes the data do not agree quite so well, but nevertheless indicate that the convection velocity is very close to the mean flow velocity on the plume centreline. The data confirm that the transition from jet-like to plume-like behaviour occurs in a rather narrow axial range.

It should be noted here that the axial measurements of concentration are inherently not as precise as the radial measurements. The reason for this is that the dye concentration drops by about 2 orders of magnitude along the imaged range as a result of dilution. Although the experimental conditions were arranged so that the effect of dilution was partly offset by the effect of beam attenuation along its traverse towards the flow nozzle, the conversion from fluorescence data to concentration data (see §3.2) required a large correction, which effectively reduced the signal-to-noise ratio at the smaller values of x. Additional difficulties arise from the severe non-uniformity in flow scales as a function of x. The decreasing resolution near the jet orifice (due to the higher fluid velocities near the flow source) inevitably introduces the 'smearing' effect discussed in §3.1. For these reasons the axial measurements were only used to obtain the average dilution along the flow axis, and not quantitative values of the higher moments of the p.d.f. as a function of x. The estimated axial convection velocities are presented, however, since it is believed that they are not affected by such an inadequacy of resolution and the data in figure 25 tend to confirm this.

5. Discussion and conclusions

5.1. *Organized mixing in the far field of buoyant jets*

The results of the present investigation show that the entrainment mechanism in the buoyant jet flow is dominated by large-scale motions. These large scales are engulfing unmixed ambient fluid and transporting it, in significant quantities, deep into regions in the flow interior where it can be subsequently mixed (molecularly) by the shearing action of smaller eddies. The instantaneous concentration pattern observed

in the flows under study shows that the entrainment mechanism cannot be viewed in terms of a 'diffusive propagation' of the interface between 'turbulent' and 'non-turbulent' fluid. In addition, our observations generally do not support any flow modelling schemes that obtain closure of the equations of motion by employing eddy-diffusivity and gradient transport concepts to problems of scalar transport and turbulent mixing. Whether such concepts can still be applied in an ensemble-average sense, as they are applicable to a Brownian motion which is also made up from discrete events is an interesting conjecture.

It is observed, on the basis of flow visualization and quantitative measurements, that both the momentum jet and the buoyancy-driven plume exhibit a periodicity associated with the passage of large-scale flow structures past the measuring station. Our observations of the momentum jet flow are in qualitative agreement with the earlier observations of Dimotakis *et al.* (1983), Zaman & Hussain (1984), and Dahm (1985). The observations of both jets and plumes suggest that the large-scale flow organization depends only on the local large length- and timescales, and not on the nature of the driving force. Despite the observed similarity in the large-scale structure of the concentration field in both jets and plumes, it is to be expected that since the flow evolution as a function of axial distance is markedly different in each case, the effect of buoyancy causes significant differences in the instantaneous concentration pattern, as well as the details of the entrainment process.

In the momentum-driven jet, a central conical region may be identified where the time-averaged local concentration is relatively uniform and generally at a higher concentration than that of the surrounding mixed fluid. At any fixed axial location, flow visualization in a transverse plane reveals that the cross-sectional area of this region changes shape in a cyclical manner, growing from an initially small region around the centre to a region encompassing the entire flow extent. Since this cyclic phenomenon, exhibiting itself in the cross-correlation functions, has a period equal to the large-scale time $T = L/U_c$, it is considered to be the signature of the large-scale structure. Similarity requires that this flow structure have the same features at any axial location as long as the driving forces are conserved. The process of entrainment is associated with the continuous engulfment of parcels of ambient fluid of various sizes from the side and back regions of these structures (viewed in a Lagrangian frame convecting with the structure). The conditional velocity measurements performed by Sreenivasan *et al.* (1979), as well as the measurements of Komori & Ueda (1985) appear to show that the large structures possess coherent vorticity in the axial direction. This vorticity would indeed cause the entrainment of ambient fluid mainly from the back regions in large 'tongues'. On the other hand, the lack of azimuthal coherence of these tongues observed from flow visualization, as in figures 1–3, appears to indicate that this axial vorticity is neither very strong nor very coherent. Visualization of plume flows in a transverse plane appear to indicate that smaller, strongly three-dimensional eddies (with vorticity vector in the radial or axial direction) are also responsible for the immediate engulfment of ambient fluid. This process may be analogous to the developed plane shear layer where, after the mixing transition, the secondary longitudinal vortex structure results in the higher values of entrainment and enhanced mixing observed by Breidenthal (1981), and Bernal & Roshko (1986).

At any axial location, the highest local concentrations are usually associated with the time instant of the arrival of a large-structure front. This was observed from digital data flow images such as in figure 7(*a*, *b*), and was demonstrated in a quantitative fashion by means of an ensemble-averaging procedure. This feature of

the jet flow is in agreement with the results of Sreenivasan *et al.* (1979) for a gas-phase momentum jet, although the concentration gradient in the axial direction is stronger in the low-*Sc* jet.

The mean local concentration at a point in space is formed in a probabilistic manner by the presence of fluid parcels at a variety of concentration levels. The range of possible concentrations in the momentum jet extends from unmixed fluid to about twice the local mean maximum value, in general agreement with the results of previous investigations. This range is considerably narrower than the range of possible concentrations in the buoyant plume.

The large-scale buoyant plume structure may be thought of as a buoyant vortex ring, with a large-scale passage periodicity scaling with L/U_c as in the momentum jet flow. This structure is observed to possess a frontal region with very high concentration, the relation of local concentration values to the local density difference, and hence to the buoyancy force, implies that the downstream region must move faster than the rest of the structure, and that the entrainment and mixing proceed primarily from the side and back side regions. It may be also suggested that pressure forces, related to the acceleration of the buoyant structure, play an increased role in bringing ambient fluid in the flow interior through the back regions. The variance in the position of arrival of a large-scale structure increases under buoyant conditions. This results in a motion that may be associated with the visually observed puffiness of the entire plume column. The large-scale plume structure seems to be structurally and dynamically similar to the buoyant ring considered by Middleton (1975) for his model of a plume cap. In this model, the entrainment into the cap takes place primarily from the rear regions.

5.2. *Effects of buoyancy on entrainment and mixing*

Dimensional arguments (Fischer *et al.* 1979) imply that the entrainment mechanism is much more efficient in the buoyancy-driven flow than in the momentum-driven flow. The present study offers an detailed view of this efficient entrainment mechanism. Flow visualization in a transverse plane reveals vortical structures of the dimension of the integral scale A with vorticity vectors along the radial direction to be active in the engulfment and molecular mixing of ambient fluid. During their roll-up, thin strained filaments with very high local concentrations are brought together with clean ambient fluid. The quantitative measurements showed that local concentration values in these strained filaments may reach values as high as 4 times the local mean maximum value. A qualitative similar mechanism is in action in the momentum jet. However, in the buoyant flow, an eddy-containing fluid emanating from the flow source will possess a dynamic of its own, as directed by its own buoyant force; therefore, it is capable of generating shear, and entraining and mixing ambient fluid. It is the interaction of a variety of such eddies with the large structure that displays the time-averaged plume behaviour. The present measurements reveal that the buoyant flow is markedly more intermittent than the momentum flow. This is associated with a more pronounced wandering of the central part of the plume column than in the jet, and with the stronger eddying motions. The higher value for the probability of detection of ambient fluid in the plume interior is intimately associated with the greater entrainment rate in the buoyant flow compared with the momentum flow. It is also responsible in part, for the high values of the r.m.s. fluctuations observed in the plume flow.

The present results indicate that the effects of buoyancy are felt primarily at scales smaller than the large scale of the flow. A direct measurement of the spatial

correlation in the concentration field reveals that buoyancy acts to decrease the degree of correlation in the direction normal to the direction of gravity. On the other hand, measurements show that scales are left largely unaffected along the direction that buoyancy forces act. Therefore, it is implied that there is a lack of homogeneity in the plume flow even at small scales, with the preferential direction being the direction of gravity. The overall effect of buoyancy is more pronounced at the small scales of the flow.

An important feature of both the momentum-driven and buoyancy-driven flows that was investigated is the strongly intermittent character of the concentration field. The intermittency of the buoyant plume is found to be very significant across the entire radial extent of the flow region. The description of transport processes by means of differential equations that utilize gradient diffusion concepts presupposes continuity of the turbulence in the entire region considered. It has been demonstrated that this is not the case, and that the deviation from such uniformity is dramatic for the buoyant flow. Therefore, it is suggested that models that incorporate the large-scale organization observed in the flow are more appropriate for the description of the transport and mixing processes.

The authors express their appreciation for the support of colleagues: Professors Donald Coles, Edward Zukoski, Paul Dimotakis and Manooch Koochesfahani, who all contributed to the initiation and evolution of this work in a variety of ways. The financial support of the National Science Foundation, through Grants No. CEE81-17272 AO1 and MSM84-12641 AO1, and the Alexander Onassis Foundation (to D. P.) are gratefully acknowledged.

REFERENCES

Antonia, R. A., Prabhu, A. & Stephenson, S. E. 1975 Conditionally sampled measurement in a heated turbulent jet. *J. Fluid Mech.* **72**, 455–480.

Batchelor, G. K. 1952 The effect of homogeneous turbulence on material lines and surfaces. *Proc. R. Soc. Lond.* A **213**, 349

Batchelor, G. K. 1959 Small scale variation of connected quantities of like temperature in turbulent fluid. Part 2. The case of large conductivity. *J. Fluid Mech.* **5**, 134–139.

Becker, H. A., Hottel, H. C. & Williams, G. C. 1967 The nozzle-fluid concentration field of the round, turbulent, free jet. *J. Fluid Mech.* **30**, 285–303.

Bernal, L. P. & Roshko, A. 1986 Streamwise vortex structure in plane mixing layers. *J. Fluid Mech.* **170**, 499–525.

Birch, A. D., Brown, D. R., Dodson, M. G. & Thomas, J. R. 1978 The turbulent concentration field of a methane jet. *J. Fluid Mech.* **88**, 431–449.

Breidenthal, R. E. 1981 Structure in turbulent mixing layers and wakes using a chemical reaction. *J. Fluid Mech.* **109**, 1–24.

Broadwell, J. E. & Breidenthal, R. E. 1982 A simple model of mixing and chemical reaction in a turbulent shear layer. *J. Fluid Mech.* **125**, 397–410.

Brown, G. L. & Roshko, A. 1974 On density effects and large structure in turbulent mixing layers. *J. Fluid Mech.* **64**, 775–816.

Chen, C. J. & Rodi, W. 1980 *Vertical Turbulent Buoyant Jets: A Review of Experimental Data.* Pergamon.

Chevray, R. & Tutu, N. K. 1978 Intermittency and preferential transport of heat in a round jet. *J. Fluid Mech.* **88**, 133–160.

Corrsin, S. & Kistler, A. L. 1955 *NACA Rep.* R-1244.

Corrsin, S. & Uberoi, M. S. 1950 Further experiments on the flow and heat transfer in a heated turbulent air jet. *NACA Rep.* 988.

DAHM, W. J. A. 1985 Experiments on entrainment, mixing and chemical reactions in turbulent jets at large Schmidt number. Ph.D. thesis, California Institute of Technology, Pasadena, California.

DEWEY, C. F. 1976 Qualitative and quantitative flow field visualization utilizing laser-induced fluorescence. *Proc. AGARD Conf. Appl. of Non-Intrusive Instrumentation in Fluid Flow Research, AGARD-CP-193.*

DIMOTAKIS, P. E., MIAKE-LYE, R. C. & PAPANTONIOU, D. A. 1983 Structure and dynamics of round turbulent jets. *Phys. Fluids* **6**, 3185.

DRAKE, M. C., PITZ, R. W. & SHYY, W. 1986 Conserved scalar probability density functions in a turbulent jet diffusion flame. *J. Fluid Mech.* **171**, 27–51.

EFFELSBERG, E. & PETERS N. 1983 A composite model for the conserved scalar PDF. *Combust. Flame* **50**, 351–360.

FISCHER, H. B., LIST, E. J., KOH, R. C. Y., IMBERGER, J. & BROOKS, N. H. 1979 *Mixing in Inland and Coastal Waters.* Academic.

HANNOUN, I. & LIST, E. J. 1988 Turbulent mixing at a shear-free density interface. *J. Fluid Mech.* **189**, 211–234.

HINZE, J. 1975 *Turbulence.* McGraw-Hill.

HUSSAIN, A. K. M. F. 1986 Coherent structures and turbulence. *J. Fluid Mech.* **173**, 303–356.

JIMENEZ, J., COGOLLOS, M. & BERNAL, L. 1985 A perspective view of the plane mixing layer. *J. Fluid Mech.* **152**, 125–143

KOMORI, S. & UEDA, H. 1985 The large-scale coherent structure in the intermittent region of the self-preserving round free jet. *J. Fluid Mech.* **152**, 337–360.

KONRAD, J. H. 1976 An experimental investigation of mixing in two-dimensional turbulent shear flows with application to diffusion-limited chemical reactions. Ph.D. thesis, California Institute of Technology, Pasadena, California. (Also *Project SQUID Tech. Rep.* CIT-8-PU.)

KOOCHESFAHANI, M. M. 1984 Experiments on turbulent mixing and chemical reactions in a liquid mixing layer. Ph.D. thesis, California Institute of Technology, Pasadena, California.

KOOCHESFAHANI, M. M. & DIMOTAKIS, P. E. 1986 Mixing and chemical reactions in a turbulent liquid mixing layer. *J. Fluid Mech.* **170**, 83–112.

KOTSOVINOS, N. E. 1977 Plane turbulent buoyant jets. Part 2. Turbulent structure. *J. Fluid Mech.* **81**, 45–62.

KYCHAKOFF, G., HOWE, R. D., HANSON, R. K. & KNAPP, K. 1983 Flow visualization in combustion gases. *AIAA Paper* 83-0405, *21st Aerospace Sciences Meeting, January 1983.*

LIST, E. J. 1982 Mechanics of turbulent buoyant jets and plumes. In *Turbulent Buoyant Jets and Plumes* (ed. W. Rodi), pp. 1–68. Pergamon.

LIU, H. T., LIN, J. T., DELISI, D. P. & ROBBEN, F. A. 1977 Application of a fluorescence technique to dye-concentration measurements in a turbulent jet. *NBS Special Pub. 484,* in *Proc. Symp. on Flow in Open Channels and Closed Conduits.*

MIDDLETON, J. H. 1975 The asymptotic behaviour of a starting plume. *J. Fluid Mech.* **72**, 753–771.

MUNGAL, M. G. & DIMOTAKIS, P. E. 1984 Mixing and combustion with low heat release in a turbulent shear layer. *J. Fluid Mech.* **148**, 349–382.

PAPANICOLAOU, P. N. & LIST, E. J. 1988 Investigations of round vertical turbulent buoyant jets. *J. Fluid Mech.* **195**, 341–391.

PAPANTONIOU, D. A. 1985 Observations in turbulent buoyant jets by use of laser-induced fluorescence. Ph.D. thesis, California Institute of Technology, Pasadena, California.

POPE, S. B. 1981 A Monte Carlo method for the PDF equations of turbulent reactive flow. *Combust Sci. Tech.* **25**, 159–174.

SAWFORD, B. L. & HUNT, J. C. R. 1986 Effects of turbulence structure, molecular diffusion and source size on scalar fluctuations in homogenous turbulence. *J. Fluid Mech.* **165**, 373–400.

SHLIEN, D. J. 1987 Observations of dispersion of entrained fluid in the self-preserving region of a turbulent jet. *J. Fluid Mech.* **183**, 163–173.

SREENIVASAN, K. R., ANTONIA, R. A. & BRITZ, K. 1979 Local isotropy and large structures in a heated turbulent jet. *J. Fluid Mech.* **94**, 745–775.

SREENIVASAN, K. R., TAVOULARIS, S. & CORRSIN, S. 1981 A test of gradient transport and its generalizations. In *Turbulent Shear Flows* 3, pp. 96–112, Springer.

TOOR, H. L. 1962 Mass transfer in dilute turbulent and non-turbulent systems with rapid irreversible reactions and equal diffusivities. *AIChE J.* **81**, 70–78.

TOWNSEND, A. A. 1976 *The Structure of Turbulent Shear Flow.* Cambridge University Press.

UBEROI, M. S. & SINGH, P. I. 1975 Turbulent mixing in a two-dimensional jet. *Phys. Fluids* **18**, 764.

WALKER, B. J. 1979 Turbulence model comparisons for shear layers and axisymmetric jets. *US Army Missile Command Tech. Rep.* RD-80-1.

WYGNANSKI, I. & FIEDLER, H. 1969 Some measurements in the self-preserving jet. *J. Fluid Mech.* **38**, 577–612.

ZAMAN, K. B. M. Q. & HUSSAIN, A. K. M. F. 1984 Natural large scale structures in the axisymmetric mixing layer. *J. Fluid Mech.* **138**, 325–351.